Vortex nucleation in phase-slippage experiments in ultrapure superfluid ^{4}He below 0.5 K

E. Varoquaux*
CNRS-Laboratoire de Physique des Solides, Université Paris-Sud, Bâtiment 510, 91405 Orsay, France

O. Avenel†
CEA-DRECAM, Service de Physique de l'État Condensé, Centre d'Études de Saclay, 91191 Gif-sur-Yvette Cedex, France
(Received 4 March 2003; published 14 August 2003)

We examine anew the problem of vortex nucleation in ultrapure ^{4}He with particular attention on the regime below 0.15 K, which is thought to involve quantum tunneling. The critical velocity data obtained in phase-slippage experiments on two samples with less than 1 ppb of ^{3}He impurities are reanalyzed so as to provide in a direct way the vortex nucleation rate. The analysis is carried out in the theoretical framework that has been developed for the escape problem of a Brownian particle from a metastable cubic potential. This theory, which has been applied successfully to superconducting Josephson junctions, gives a fully consistent account of the experimental observations in both the temperature-dependent regime above 0.15 K and the low-temperature plateau.

DOI: 10.1103/PhysRevB.68.054515 PACS number(s): 67.40.Hf, 67.40.Vs

I. INTRODUCTION

As Feynman suggested in 1954,[1] vortices are believed to be formed when superfluid ^{4}He is forced to flow through a constriction and its superfluid property is destroyed. For critical flow through submicron-size apertures, vortex formation takes place according to a scenario in which vortex half rings nucleate at the wall of the aperture, at a site where the local superfluid critical velocity v_c is exceeded.[2–7] In larger channels, more complicated hydrodynamical processes come into play, leading to the formation of self-sustained vortex tangles and turbulent flows.[8] Some of the many phenomena arising from the dynamics of quantized vorticity in superfluids are described in a recent book edited by Barenghi, Donnelly, and Vinen.[9]

Here, we restrict our scope to the formation of vortices one by one in aperture flow. We present an analysis of the experimental data on phase slippage in ultrapure ^{4}He at temperatures from $\sim$400 mK down to 17 mK already reported in Refs. 4 and 10. This more detailed analysis brings into better focus the observations that have laid the experimental ground work for the half-ring scenario. Some pending issues on quantum tunneling of vortices of mesoscopic sizes are reexamined in greater depth in light of these more precise results.

The vortex nucleation problem has been considered from the theoretical point of view by, in particular, Iordanskii,[11] Langer and Fisher,[12] Volovik,[13] Muirhead *et al.*,[14] Sonin,[15,16] Fischer,[17,18] and others (see, for instance, Ref. 5 for more references). The description of a vortex involves few macroscopic variables, and one only–the radius—in the case of a circular, or semicircular, vortex. The problem can thus be modeled by the escape of a particle confined in a metastable potential. For vortex rings, or half rings, the well is one dimensional as pictured in Fig. 1.

Two regimes in temperature are distinguished. At high temperature, the particle can be thermally excited to an energy above the top of the potential barrier and fall down on the continuum side. The inverse decay time for such a process, that is, the number of events per unit time Γ, is expressed by the Arrhenius law

$$\Gamma_A = \frac{\omega_0}{2\pi} \exp\left\{ -\frac{E_b}{k_B T} \right\}. \tag{1}$$

The attempt frequency $\omega_0/2\pi$ characterizes the dynamics of the system; the energy barrier E_b is the depth of the potential well.

As T decreases, the rate (1) becomes vanishingly small and, quantum mechanics prevailing, the particle escapes by tunneling under the potential barrier at a rate that can be expressed in the Wentzel-Kramers-Brillouin approximation as $A \exp(-S/\hbar)$, S being the action of the particle along the saddle-point trajectory at the top of the potential barrier, the so-called ''bounce.'' Full expressions for Γ in the various regimes are given below. The crossover from thermal activation to quantum tunneling takes place close to the temperature at which the rates are equal, $T_0 \sim \hbar\omega_0/2\pi k_B$.[19,20]

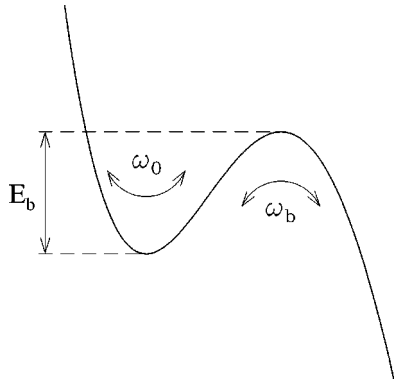

FIG. 1. Potential well trapping a particle in one dimension. The particle can escape to the continuum of states to the right. The lowest mode at the bottom of the well has angular frequency ω_0; ω_b would be the corresponding quantity if the potential was inverted bottom over top.

Fully documented cases of macroscopic quantum tunneling are few. Definitive work has only been conducted on artificial structures, namely, electrodynamic Josephson junctions,[21] but most mesoscopic structures that form at low temperature, including helium vortices, can possibly quantum tunnel out of their confining potential.

Our purpose here is to show that the experimental data on phase slippage in ultrapure ^{4}He at low temperature can be interpreted in their very details in a model in which vortices are nucleated by quantum tunneling. We first summarize the theoretical results for the escape of a Brownian particle (Sec. II). We next lay the ground work for the statistical analysis of the experimental observations in a detailed and complete manner in order to clearly distinguish the various, nonequivalent approaches that have been used in previous work (Sec. III). The outcome of this analysis is given in Sec. IV. Finally, we state how these results provide support for the nucleation model, compare the various ways to derive values for the energy barrier from the data, and discuss the influence of damping, which, albeit small, can be estimated from the data (Sec. V). We summarize our work in Sec. VI.

II. ESCAPE OF A BROWNIAN PARTICLE FROM A WELL

Expression (1) assumes thermal equilibrium, that is, some degree of interaction of the particle with a heat bath. The particle is thus subject to random forces, experiences friction, and undergoes Brownian motion. Following the pioneering approach of Kramers,[22] the escape from a well of such a Brownian particle has been considered in particular by Langer[23] in the classical, thermally activated regime, and by Caldeira and Leggett[24] in the quantum regime. At temperatures where the thermal energy is large with respect to the well depth, the escape process results from the inelastic scattering of thermal excitations by the metastable particle while quantum tunneling is a manifestation of the zero-point fluctuations in the environment.[25]

Thermal activation and quantum tunneling are well-established phenomena for microscopic systems. How the quantum regime goes over to mesoscopic systems, which involve a large number of coupled microscopic components and in which the effect of the environment affects quantum tunneling, has been considered by Caldeira and Leggett[24] and a number of other workers (for general reviews, see Refs. 26–29). Most of these studies were devoted to superconducting Josephson devices (see, in particular, the reviews by Larkin, Likharev, and Ovchinnikov[26] and by Grabert[27]) and are remarkably well confirmed by experiments, in particular:[30–33] that quantum tunneling can take place in such large systems is a well-established experimental fact.[21]

Hosts of other mesoscopic systems are thought to exhibit quantum-tunneling phenomena, for instance, charge-density waves in quasi-one-dimensional conductors,[34,35] vortices in superconductors,[36,37] vortices and spin domains in Bose-Einstein condensates,[38,39] cavitation of bubbles in helium,[40–42] crystalization in ^{4}He,[43] magnetic clusters.[44,45] They are also believed to occur in the nucleation of superfluid vortices, both in ion propagation[46,47] and in orifice flow,[10,13,16–18,48,49] as well as for vortices in cosmology.[50]

In all these last instances, the evidence stemming from experiments is less convincing and the applicability of theory conveys less confidence than that for the Josephson devices. Some of the difficulties which arise in the case of vortices in fermionic systems have been brought forward by Volovik.[51] In the superfluid case, the energy spectrum of vortices has a gap,[52,53] since extremely small vortices do not even exist. Also, angular momentum is conserved: it is difficult to envision vorticity spinning out of thin air into an already sizable hydrodynamical object carrying one quantum of circulation.

However, as we have previously stated,[4,10,54,55] the experimental observations of the critical velocity in aperture flow and of its fluctuations in ultrapure ^{4}He at very low temperature are fully accounted for by thermal activation at temperatures above ~ 0.12–0.15 K, and by quantum tunneling below. Redundancy in the experimental data allows to check the energy barrier values extracted below and above the observed crossover temperature against one another. The case for a crossover from thermal to quantum vortex nucleation appears well borne out by experiments.

Before turning to the detailed analysis of the critical velocity measurements, from which this conclusion is derived, we give a brief account of the theory of the escape of a particle from a metastable state in a potential well to a continuum of states.

A. Thermal escape

The escape process is governed by the shape and height of the potential barrier, pictured in Fig. 1, by the mass of the particle, and by the interaction with an environment which acts as a thermal bath. The theoretical problem of the escape rate of such a Brownian particle has been reviewed by a number of authors, in particular in Refs. 27–29, 56, and 57. Below, we follow mainly the work of Grabert *et al.*[27,56]

The effect of dissipation on the Arrhenius rate, Eq. (1), has first been evaluated by Kramers[22] in the case of a frequency-independent damping corresponding to a white-noise spectrum. This type of friction, referred to as Ohmic damping, has been studied extensively as it applies to resistively shunted Josephson devices. It may not necessarily be the most relevant to vortex nucleation in superfluids but it does account in an approximate manner for the dissipation associated with the radiation of phonons that accompanies the sudden appearance and growth of vortices during nucleation, and, at nonzero temperature, with the interaction with the normal fluid (here, thermally excited phonons). As shown below, damping is weak in superfluid ^{4}He below 0.5 K, as can be expected, and extremely weak below 0.1 K. Dissipation is characterized by a dimensionless coefficient $\alpha = 1/2\omega_b\tau$, τ being the time of relaxation of the system toward equilibrium.

According to Kramers[22] (see, e.g., Hänggi *et al.*[28]) the effect of damping on the escape rate in the thermally activated (classical) regime is to modify the prefactor in Eq. (1):

$$\Gamma_{\mathrm{K}} = \frac{\omega_0}{2\pi}\left[(1+\alpha^2)^{1/2} - \alpha\right]\exp\left\{-\frac{E_b}{k_{\mathrm{B}}T}\right\} \quad . \tag{2}$$

For Eq. (2) to hold, thermal equilibrium must be established, which requires that $E_b \gg k_B T \gg \hbar\omega_0$, namely, escape must be infrequent. This condition is not verified close to the lability point at which E_b vanishes. Also, damping cannot be too small otherwise the system is in effect isolated from the environment. For vortex nucleation in helium, both conditions would be violated at very low temperature, but, as will be seen below, quantum fluctuations take over and change the picture.

The gradual onset of quantum fluctuations as the temperature is lowered comes in as additional assistance to nucleation while thermal fluctuations become weaker: the thermal activation rate (2) is multiplied by a factor $f_{\rm th}$, which is expressed for frequency-independent (Ohmic) damping by

$$\Gamma_{\rm th} = f_{\rm th}\Gamma_{\rm K}, \tag{3}$$

$$f_{\rm th} = \frac{\Gamma(1-\mu_b^+/\theta)\Gamma(1-\mu_b^-/\theta)}{\Gamma(1-\mu_0^+/\theta)\Gamma(1-\mu_0^-/\theta)},$$

in which

$$\theta = 2\pi k_B T/\hbar\omega_0,$$

$$\mu_b^{\pm} = -\alpha \pm (1+\alpha^2)^{1/2},$$

$$\mu_0^{\pm} = -\alpha \pm i([\omega_0^2/\omega_b^2]-\alpha^2)^{1/2}.$$

The quantities μ_0^+ and μ_0^- are complex conjugates and the product of the Γ functions in the denominator of Eq. (3) is real. The quantum correction factor $f_{\rm th}$ goes to 1 in the high-temperature limit, and, to leading order in $1/T$, is independent of damping:

$$f_{\rm th} = \exp\left\{\frac{\hbar^2}{24}\frac{(\omega_0^2+\omega_b^2)}{(k_B T)^2} + \mathcal{O}(\alpha/T^3, 1/T^4)\right\}. \tag{4}$$

Equation (3) diverges as $\theta \to \mu_b^+$ because $\Gamma(1-\mu_b^+/\theta)$ diverges since its argument goes to zero. This mathematical singularity is of no physical consequence since another channel for nucleation opens up in its vicinity, that of quantum tunneling. The crossover temperature in the presence of dissipation is defined by the opening of the new channel at $\mu_b^+ = \theta$:

$$T_0 = \hbar\omega_b[(1+\alpha^2)^{1/2}-\alpha]/2\pi k_B. \tag{5}$$

Equation (3) remains valid down to temperatures quite close to T_0 as thermal fluctuations overtake quantum fluctuations in an exponential manner—the Boltzmann factor in Eq. (2)—in systems weakly coupled to their environment.

B. The quantum region

Below T_0, quantum tunneling takes over. The full quantum regime sets in rapidly in the case of weak to moderate damping since thermal fluctuations die out exponentially as T decreases. Actually, there exists around T_0 a crossover region where neither thermal fluctuations nor quantum fluctuations dominate and where both contribute to the escape process but this region is very narrow for weak to moderate damping.

The quantum-tunneling rate is governed by the action of the tunneling particle along the minimal-action path over a saddle point of the confining potential, which depends on the detailed shape and spatial extent of the potential well. We consider below a simplified form for this potential and justify its use. In the problem at hand here, the potential barrier is controlled by the flow velocity past the obstacle about which vortices nucleate: the higher the velocity, the smaller and narrower the barrier E_b until, eventually, it becomes so small that the nucleation rate becomes very high; vortices nucleate very readily at high flow velocities. This lability property has been shown to exist in numerical simulations using the Gross-Pitaevski equation.[53,58,59]

Consider the analytic potential $V(q)$ pictured in Fig. 1. It can be represented by the first terms of the Taylor expansion about the well bottom, taken to be at $q=0$

$$V(q) = V_0 + \frac{1}{2}\left.\frac{\partial^2 V}{\partial q^2}\right|_{q=0} q^2 + \frac{1}{6}\left.\frac{\partial^3 V}{\partial q^3}\right|_{q=0} q^3 + \ldots.$$

If terms of order higher than 3 can be neglected, which is the case close to the lability point at which q_b and $E_b = V(q_b) - V(0)$ vanish, the barrier top lies at

$$q_b = -2\left.\frac{\partial^2 V}{\partial q^2}\right|_{q=0} \Big/ \left.\frac{\partial^3 V}{\partial q^3}\right|_{q=0},$$

so that the potential reduces to the so-called ''cubic'' well

$$V(q) = V_0 + \frac{m}{2}\omega_0^2 q^2\left(1 - \frac{2q}{3q_b}\right). \tag{6}$$

The angular frequency of the particle oscillations at the bottom of the well is $\omega_0 = [(1/m)\partial^2 V/\partial q^2|_{q=0}]^{1/2}$, m being the particle mass. It is easily seen that $\omega_b = -[(1/m)\,\partial^2 V/\partial q^2)|_{q=q_b}]^{1/2} = \omega_0$. The ''cubic'' potential, which represents the general form of analytic potentials close to the lability point, involves only one characteristic frequency.

The rate at which a Brownian particle escapes by quantum tunneling from such a cubic potential has been calculated explicitly. In the case of weak Ohmic damping ($\alpha \ll 1$), this rate takes the form[24,56,57]

$$\Gamma_{\rm qt} = \frac{\omega_0}{2\pi}\left(864\pi\frac{E_b}{\hbar\omega_0}\right)^{1/2}\exp\left\{-\frac{36}{5}\frac{E_b}{\hbar\omega_0}\left[1+\frac{45\zeta(3)}{\pi^3}\alpha\right] + \frac{18}{\pi}\alpha\frac{T^2}{T_0^2} + \mathcal{O}\left(\alpha^2, \alpha\frac{T^4}{T_0^4}\right)\right\}. \tag{7}$$

The Riemann number $\zeta(3) = 1.202\,05\ldots$. Damping both decreases the zero-temperature escape rate and introduces a temperature dependence to the quantum regime. Equation (7) is accurate only below $T_0/2$ and for low α. Grabert *et al.*[56] have given numerical tables to compute the rate up to $\sim T_0$

when Eq. (7) fails. This temperature range is found particularly relevant in the following.

In the immediate vicinity of T_0, neither Eq. (7) nor Eq. (2) supplemented by Eq. (4) yield good estimates of the escape rate. Either the numerical tables of Grabert *et al.*[56] or the following closed-form asymptotic expression of the rate valid in the crossover region about T_0 for Ohmic damping and a cubic potential (see also Hänggi, Talkner, and Borkovec[28]) can then be used:

$$\Gamma_{\rm co} = f_{\rm co}\Gamma_{\rm K},$$

$$f_{\rm co} = \left(\frac{\pi r E_b}{\hbar\omega_0}\right)^{1/2} \theta_0 \frac{\Gamma(1-\mu_b^-/\theta_0)}{\Gamma(1-\mu_0^+/\theta_0)\Gamma(1-\mu_0^-/\theta_0)} \times \mathrm{erfc}(u)\exp(u^2) \tag{8}$$

in which

$$\theta_0 = 2\pi k_{\rm B}T_0/\hbar\omega_0 = (1+\alpha^2)^{1/2}-\alpha,$$

$$r = 12\pi\frac{1+\alpha^2}{\theta_0}\frac{1+2\theta_0^2}{1+4\theta_0^2},$$

$$u = \left(\frac{rE_b}{\hbar\omega_0}\right)^{1/2}(\theta-\theta_0),$$

and $\mathrm{erfc}(x)$ is the complementary error function. The validity of Eq. (8) is limited to the temperature range $|u| \lesssim 1$.

A numerical evaluation of Eqs. (3) and (4) shows that quantum fluctuations affect the thermal activation process at temperatures as high as $3T_0$, depending on damping, and become dominant when Eq. (8) takes over. In the crossover region, the barrier is traversed by a combination of thermal activation part way up the well and of quantum tunneling through the part of the barrier that has not been surmounted. The quantities $f_{\rm th}$ and $f_{\rm co}$ join in a nearly smooth manner; the resulting (numerical) combination will be denoted $f_{\rm q}$ in the following.[60]

C. The depopulation factor

For Kramers' expression (2) of the thermally assisted escape rate $\Gamma_{\rm K}$ to hold, the Brownian particle must be in thermal equilibrium with its environment. In particular, damping must not be vanishingly small. Kramers also discussed in 1940 (Ref. 22) the limit of very small damping in which energy levels are not populated according to the Boltzmann factor in Ref. 2 but the full turnover problem from vanishing damping to intermediate and large damping was solved only in the 1980s.

Grabert[61] first worked out a proper formulation in the classical regime ($T \gg T_0$) in terms of the normal modes of the coupled system formed by the metastable particle and the thermal bath,[62] and, more specifically, the unstable mode with frequency $\omega_b[(1+\alpha^2)^{1/2}-\alpha]$. The extension to the temperature range $T \gtrsim T_0$ was then carried out by Rips and Pollak[63] who showed that the rate for arbitrary damping in the temperature range $T > T_0$ can be factorized into physically meaningful terms:

$$\Gamma = \frac{\omega_0}{2\pi}[(1+\alpha^2)^{1/2}-\alpha] f_{\rm q} \Upsilon \exp\left\{-\frac{E_b}{k_{\rm B}T}\right\}, \tag{9}$$

namely, the classical Kramers rate $\Gamma_{\rm K}$, the quantum correction factor $f_{\rm q}$, and the depopulation factor Υ, which is unity at large α and decreases to zero as $\alpha \to 0$.

For a cubic potential with Ohmic dissipation, the depopulation factor is expressed by[63]

$$\ln\Upsilon = \frac{z}{2\pi}\sin\left(\frac{z}{2}\right)\int_{-\infty}^{\infty} d\tau \frac{\ln\left\{1-\exp\left[-\frac{27\pi}{4}\left(1+\frac{1}{\mu}\right)^3(\mu^2-1)I(\tau,\mu;z)\frac{E_b}{k_{\rm B}T}\right]\right\}}{\cosh(\tau z)-\cos(z/2)}, \tag{10}$$

with

$$I(\tau,\mu;z) = \int_0^\infty dy \frac{y^4(y^2+1)}{(y^2+\mu^2)\sinh^2(\pi y)}\frac{\cosh(zy/2)-\cos(\tau z y)}{(zy/2)\sinh(zy/2)},$$

$$\mu = \frac{(1+\alpha^2)^{1/2}+\alpha}{(1+\alpha^2)^{1/2}-\alpha}, \quad z = \frac{2\pi T_0}{T}.$$

According to Rips and Pollak,[63] below T_0 the particle does not need energy from the bath to tunnel through the barrier: Υ is taken to be unity.

This theoretical description of the escape of a Brownian particle has been compared to the behavior of actual systems, Josephson devices.[30,32,33,64,65] The study of these man-made devices, in which various parameters including dissipation can be tuned externally, has brought forward particularly convincing experimental checks of the existence of quantum collective variables that exhibit quantum tunneling, of the reality of quantum tunneling in macroscopic systems, and of the effect of dissipation on macroscopic quantum tunneling.[21] As stated above, other physical systems, vortices in superconductors and in helium, and bubble cavitation in helium, are also believed to undergo macroscopic quantum tunneling, i.e., their behavior can be likened to that of a Brownian particle in a well.

Given a particular system characterized by an energy barrier E_b, a ground-state energy $\hbar\omega_0$, and a damping parameter α, the escape rate can easily be evaluated numerically

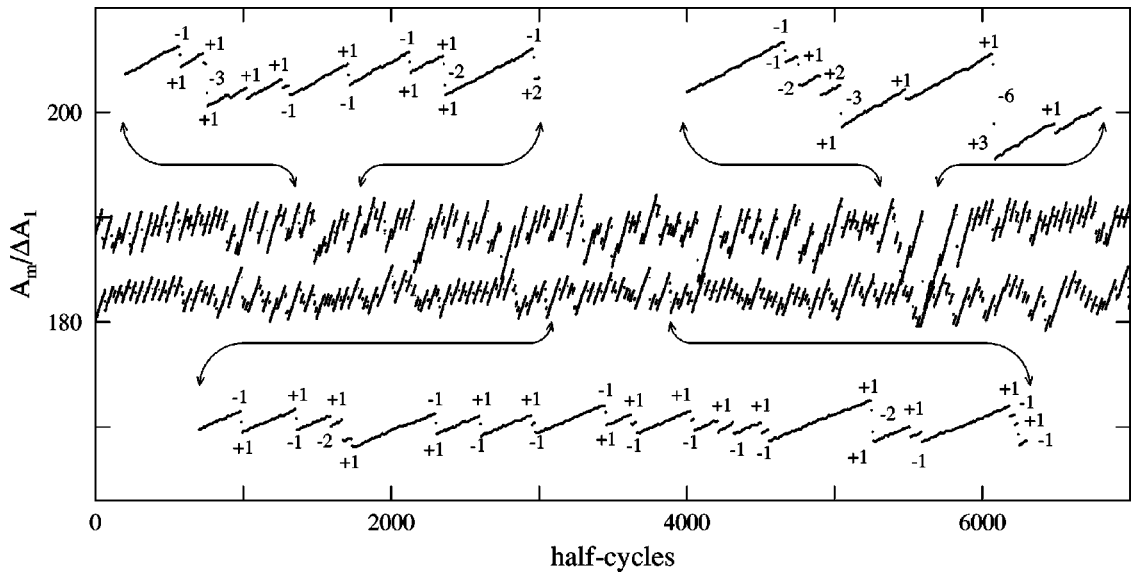

FIG. 2. Peak amplitude charts at 100.7 mK (top) and 201.5 mK (bottom). Peak absolute amplitudes during each half-cycle are plotted as a function of half-cycle index; time runs from left to right. The peak membrane amplitude A_m is normalized to the amplitude jump of a single slip ΔA_1. The expanded traces at the very top and bottom of the graph show the slip sizes in signed winding numbers (according to flow direction, in and out of the resonator chamber).

from expressions (3), (7), (8), and (9) and the numerical tables in Ref. 56 over the whole range of temperature with modest computing power. Our task, however, is to work backward and, from the knowledge of the experimental escape rate and the critical velocity at various temperatures, to find $E_b(v)$, $\hbar\omega_0$, and α. This task is performed in a number of iterative steps. Before we begin, we need to expound the different ways of analyzing the raw data and to find the least biased one to obtain the experimental nucleation rate.

III. THE DATA ANALYSIS

A. The raw experimental data

Experiments were conducted in a miniature hydromechanical device, which is basically a flexible-diaphragm Helmholtz resonator. This resonator is immersed into a bath of superfluid. The flexible diaphragm is constituted by a Kapton membrane coated with aluminum. There are two openings connecting the resonator chamber to the superfluid bath. One is a microaperture in which the critical velocity phenomenon takes place. The critical event consists of a sudden jump in the resonance amplitude which corresponds to an abrupt change in the flow velocity through the microaperture and a loss of resonator energy. These dissipation events are interpreted as resulting from single vortex emission, to which is associated a slip by 2π of the quantum phase difference across the microaperture $\delta\varphi$ caused by the motion of the vortex across the flow stream.

The other opening is a relatively open duct and provides to the superfluid a parallel path along which the quantum phase remains well determined. A quantum of circulation, $\kappa_4 = 2\pi\hbar/m_4$, m_4 being the mass of a ^{4}He atom, builds up for each 2π slip along the superfluid closed loop threading the two openings. A fraction $1/(1+R)$ of the total volume of fluid displaced by the membrane flows through the microaperture, with $R/(1+R)$ flowing through the parallel channel; R is the ratio of the classical hydraulic inductances of the two openings. The operation of these resonators is described in detail in the literature (see, for instance Refs. 5 and 66–69).

The resonator is driven on resonance with an electrostatic ac drive at a fixed level. In the absence of dissipation, the resonance motion increases linearly in amplitude under the action of the drive. The displacement of the membrane, which is proportional to the total flow in and out of the resonator, is monitored by a superconducting quantum interference device, the output of which is converted into a digital signal by a fast analog-to-digital converter. We monitor the peak amplitude of the membrane motion A_m at each half cycle of the resonance. The peak amplitude data points are stored digitally in real time. The raw data consist of peak amplitude charts as represented in Fig. 2. Phase slips are seen as sudden drops of the peak amplitude from one half cycle to the next. An amplitude chart typically consists of a record of 32 640 peak amplitude measurements, spanning a lapse of time of 16 320 periods of the resonance, typically 20 min, and containing from several hundreds to several thousands of slips depending on the drive power. Temperature is measured by a Speer resistor calibrated against a NMR platinum thermometer.

The pattern of these peak amplitude data is processed numerically to identify all the slips and their multiplicity, and to obtain the state j of the quantized circulation trapped in the resonator loop. The actual flow in the microaperture is the sum of the flow driven by the membrane and of the persistent flow threading the microaperture and the parallel channel, which depends on the quantum state of the loop j.

The amplitude drop ΔA_1 caused by a single phase slip in a given half cycle of the resonance corresponds to a change of $\delta\varphi$ by exactly 2π. Normalizing the membrane displacement A_m by ΔA_1, a quantity which is readily read off the

peak amplitude charts, provides a self-calibration of the data which is independent of less well-known quantities such as the membrane stiffness and hydraulic area, the aperture geometry, and the calibration factor of the displacement sensor. The peak aperture velocity v_p is deduced from the peak membrane amplitude and from the trapped circulation by[69,70]

$$v_p = \frac{A_m}{\Delta A_1 (1+R)} + \left(j + \frac{\kappa_b}{\kappa_4} \right) \frac{R}{1+R}. \tag{11}$$

In Eq. (11) and in the following, aperture velocities are expressed by the (fractional) number of turns $\delta\varphi/2\pi$ by which the quantum-mechanical phase winds across the aperture. The actual flow velocity averaged over the cross section of the microaperture is proportional to $\delta\varphi$, the multiplying factor being $\hbar/m_4 l_{\mathrm{H}}$. The hydraulic length l_{H} of the microaperture is of the order of 1 μm in the present experiments.

The experimental parameters such as κ_b, the circulation in the loop which arises from remanent vorticity or applied rotation,[71] ΔA_1, the amplitude drop of a single slip, δv_d, the increase in peak velocity from one half cycle to the next due to the drive, and R, the ratio of the hydrodynamic inductances of the two openings (3.90 in the experiments on ultrapure helium), can be derived self-consistently with great accuracy from the full analysis of the peak amplitude charts.[69,71]

The velocity at which phase slips occur is a stochastic quantity, the value of which differs slightly from one event to the next. The analysis of the raw data outlined above provides sets of values, or slip velocity records, for these events. These variations are caused by the statistical properties of vortex formation; the background noise of the measuring apparatus, the hydromechanical resonator, is due mainly to mechanical vibrations and is significantly lower than phase-slip noise. Some uncertainty also arises from the analysis of the statistical properties of the phase-slip data. In view of the different methods of analysis which have been used,[72–74] we give in full the definitions of the different statistical quantities which have been introduced and compare them in detail below.

B. The probability of nucleation events

We start from the records of the velocities at which the critical events have been taking place and we proceed to consider the probability distribution of the nucleation process. From this quantity, we define the actual critical velocity v_c for phase slips and the statistical width of the critical transition Δv_c. We follow Refs. 4 and 72. The quantities are directly related to E_b, ω_0, and α and can readily be extracted from the records of the critical events, as we show below.

The energy barrier E_b depends on the local fluid velocity at the nucleation site, which is the control parameter for nucleation. It may also be expected on dimensional grounds that E_b is proportional to the (superfluid) density ρ_s which itself is a function of temperature, pressure, and velocity. The superfluid coherence length can also be expected to enter the problem. Isotopic impurities are known to strongly affect phase-slip nucleation and their effect is largely understood.[75] Here we are mainly concerned with ultrapure ^{4}He containing less than 10^{-9} of ^{3}He impurities, at pressures close to saturated vapor pressure (SVP) and at temperatures ranging from 18 to 400 mK. Only the temperature and velocity dependencies are studied here.

Let us denote the (Poissonian) probability to observe a slip in a given time interval dt at a given flow velocity v by $\Gamma(T,v)\,\mathrm{d}t$. The differential probability d$p(t)$ that a slip takes place during the time interval dt at the specified time t of the resonance motion is the product of the probabilities of the two statistically independent events that (i) no slip has taken place before time t, and (ii) a slip takes place during dt:

$$\mathrm{d}p = [1 - p(t)]\,\Gamma(T,v)\,\mathrm{d}t. \tag{12}$$

Integrating Eq. (12) from t_i to t_f yields the probability that a slip has taken place in the time interval $t_f - t_i$:[76]

$$p = 1 - \exp\left\{ - \int_{t_i}^{t_f} \Gamma[T, v_p \cos(\omega t')]\,\mathrm{d}t' \right\}. \tag{13}$$

The sinusoidal time dependence of the velocity in Eq. (13) follows from the fact that the resonator in which these phase-slip experiments are conducted has a high quality factor and is weakly perturbed by the external drive: in the absence of phase slips, its steady-state motion is purely sinusoidal at angular frequency ω. The peak value reached by the velocity at each half cycle is v_p. The actual motion in the presence of slips has been analyzed in detail in Ref. 69: it is a pure sine before (and after) the slip. The time evolution of the velocity is therefore taken as $v_p \cos(\omega t)$ in expression (13) for $p(t)$.

The rate at which slips occur in the various regimes of fluctuations, thermal, quantum, or mixed is given, as described in Sec. II, by Eqs. (3), (7), or (8), which we write for short in this section as

$$\Gamma(T,v) = \Gamma_0 \exp\{-E_a/k_{\mathrm{B}}T\}, \tag{14}$$

in which the prefactor reads

$$\Gamma_0 = \omega_0 [(1+\alpha^2)^{1/2} - \alpha]/2\pi,$$

$$\Gamma_0 = \omega_0 [864\pi E_b/(\hbar\omega_0)]^{1/2}/2\pi$$

and the exponent reads

$$\frac{E_a}{k_{\mathrm{B}}T} = \frac{E_b}{k_{\mathrm{B}}T} - \ln(f_q \Upsilon),$$

$$\frac{E_a}{k_{\mathrm{B}}T} = \frac{36}{5}\frac{E_b}{\hbar\omega_0}\left[1 + \frac{45\zeta(3)}{\pi^3}\alpha\right] - \frac{18}{\pi}\alpha\frac{T^2}{T_0^2} + \cdots$$

in the thermal regime down to slightly below T_0 (to the limit of the validity of f_{q}), and the deep quantum regime, respectively. The numerical tables in Ref. 56 must be used to bridge the gap between the crossover regime and the deep quantum regime. In this way, all temperature regimes can be treated formally on the same footing, the generalized activation energy E_a including the full quantum corrections.

The time integral in Eq. (13) can be evaluated to asymptotic accuracy by the method of steepest descent.[77] We

perform the integration over a half cycle of the resonance and find the expression of the probability that a phase slip takes place in a given half cycle in which the superfluid velocity reaches the peak value v_p:

$$p(v_p)=1-\exp\left\{-\frac{\Gamma_0}{\omega}\sqrt{\frac{-2\pi k_B T}{v_p \partial E_a/\partial v|_{v=v_p}}}\exp\left[-\frac{E_a(v_p)}{k_B T}\right]\right\}. \tag{15}$$

The critical velocity v_c associated with the nucleation process is defined as the velocity for which $p(v_c)=\frac{1}{2}$. The implicit equation yielding v_c reads

$$\frac{\Gamma_0}{\omega}\sqrt{\frac{-2\pi k_B T}{v_c \partial E_a/\partial v|_{v_c}}}\exp\left\{-\frac{E_a(v_c)}{k_B T}\right\}=\ln 2. \tag{16}$$

It follows from Eqs. (14) and (16) that the nucleation rate at v_c, Γ_c, is given by

$$\Gamma_c=(\omega \ln 2)\sqrt{\frac{v_c \partial E_a/\partial v|_{v_c}}{-2\pi k_B T}}. \tag{17}$$

The actual velocity at which each critical event takes place is a stochastic quantity which departs slightly from v_c; its spread is characterized by the ''width'' of the probability distribution Δv_c defined[3,4] as the inverse of the slope of the distribution $p(v)$ at v_c, $(\partial p/\partial v|_{v_c})^{-1}$. This derivative can be expressed as follows, assuming that Γ_0 does not depend on v:

$$\frac{\partial p}{\partial v}=-\frac{\Gamma(T,v)}{\omega}[1-p]\sqrt{\frac{-2\pi k_B T}{v\,\partial E_a/\partial v}} \times\left\{\frac{1}{2}\left[\frac{1}{v}+\frac{\partial^2 E_a}{\partial v^2}\Big/\frac{\partial E_a}{\partial v}\right]+\frac{1}{k_B T}\frac{\partial E_a}{\partial v}\right\}.$$

The critical width at v_c, setting $p=\frac{1}{2}$ and using Eq. (16), finally can be written as

$$\Delta v_c=\left(\frac{\partial p}{\partial v}\bigg|_{v_c}\right)^{-1} =-\frac{2}{\ln 2}\left[\frac{1}{k_B T}\frac{\partial E_a}{\partial v}\bigg|_{v_c} +\frac{1}{2}\left\{\frac{1}{v_c}+\frac{\partial^2 E_a}{\partial v^2}\bigg|_{v_c}\Big/\frac{\partial E_a}{\partial v}\bigg|_{v_c}\right\}\right]^{-1}. \tag{18}$$

At low temperatures and large critical velocities, the quantity in curly brackets on the right hand side (rhs) of Eq. (18) is small with respect to the first term so that Eq. (18) simplifies to

$$\Delta v_c=-\frac{2}{\ln 2}k_B T\left(\frac{\partial E_a}{\partial v}\bigg|_{v_c}\right)^{-1}. \tag{19}$$

Equation (19) relates, within its range of validity, Δv_c to the slope of the energy barrier at v_c. The minus sign comes from the fact that the energy barrier E_a decreases as v increases; the width Δv_c is defined as a positive quantity.

As defined above, v_c and Δv_c are directly related to the activation energy and are independent of the drive level. They depend logarithmically on the resonator frequency $\omega/2\pi$, which reflects the fact that the observation of a phase slip involves a characteristic time depending on the measuring apparatus as discussed in Ref. 78.

C. Apparent critical velocity and width

The apparent critical velocity v_a is the arithmetical mean of the peak velocities at which the slips occur. The harder the resonator is excited by the external drive, the higher will be this mean value. The quantity v_a is very readily obtained from slip data records. The root-mean-square deviation of the slip velocities with respect to the mean is Δv_a. The values of v_a and Δv_a are related to the nucleation velocity v_c and width Δv_c defined in the previous section in a manner which we now derive.

Let us consider the situation met in the present experiments where the resonator is driven with a fixed ac-voltage level and where its peak amplitude increases (linearly) from half cycle to half cycle by δv_d for a number of half cycles before a slip occurs. The probability for a slip to occur during a half cycle with peak velocity v_p is given by Eq. (15). The probability density $f(v_p)$ that a slip takes place during the half cycle with amplitude v_p, the resonator starting from rest, is expressed as the product of the probability of a slip during the half cycle under consideration multiplied by the probability that the slip did not take place at previous half cycles:

$$f(v_p)=p(v_p)[1-p(v_p-\delta v_d)][1-p(v_p-2\delta v_p)]\ldots. \tag{20}$$

Using Eqs. (15) and (17), we can rewrite Eq. (20) as

$$f(v_p)=p(v_p)\exp\left\{-\frac{\Gamma_0 \ln 2}{\Gamma_c} \times\sum_{n=1}^{N}\exp\left[\frac{-E_a(T,P,v_p-n\delta v_d)}{k_B T}\right]\right\}, \tag{21}$$

where N is the number of the previous half cycles during which no slip occurred. In the above, we have taken into account that phase slips become probable only when v_p is close to v_c, and that the peak amplitude increment δv_d is small with respect to v_p. This last condition ensures, in particular, that the drive applied to the resonator is not strong to the extent of distorting the sinusoidal resonance motion. We further assume that δv_d is not vanishingly small so that the probability $f(v)$ becomes independent of N for N moderately large. The range of validity of our derivation is thus limited to experimental situations in which phase slips occur on the average every few resonance cycles, as is the case for the data represented in Fig. 2. Finally, Γ_0 is taken independent of v in the derivation of Eq. (21).

To proceed with the evaluation of Eq. (21), we note that the probability distribution $f(v_p)$ and the probability $p(v_p)$ exhibit an extremely strong dependence on v_p while the activation energy E_a is a moderately rapidly varying function of v_p. The following expansion of E_a about v_p,

$$E_a(v_p - n\,\delta v_d) \simeq E_a(v_p) - \left.\frac{\partial E_a}{\partial v}\right|_{v_p} n\,\delta v_d,$$

covers a large span of variation for Eq. (21) and is accurate enough for our purpose. We then rewrite Eq. (21) as

$$f(v_p) = p(v_p)\exp\left\{-\ln 2\frac{\Gamma_0}{\Gamma_c}\exp\left[-\frac{E_a(v_p)}{k_B T}\right] \times \sum_{n=1}^{N}\exp\left[n\frac{\delta v_d}{k_B T}\left.\frac{\partial E_a}{\partial v}\right|_{v_p}\right]\right\}, \tag{22}$$

and we express the peak velocity v_p in terms of the critical velocity v_c and a small deviation δv, $v_p = v_c + \delta v$, in order to use Eqs. (17) and (19) to simplify Eqs. (15) and (22):

$$\begin{aligned} p(v_p) &= 1 - \exp\left(-\ln 2\frac{\Gamma_0}{\Gamma_c}\exp\left\{-\frac{1}{k_B T} \times \left[E_a(v_c) + \left.\frac{\partial E_a}{\partial v}\right|_{v_c}\delta v\right]\right\}\right) \\ &= 1 - \exp\left\{-\ln 2\exp\left(\frac{2}{\ln 2}\frac{\delta v}{\Delta v_c}\right)\right\} \\ &= 1 - \exp\{-\ln 2\, e^z\}, \end{aligned} \tag{23}$$

$$\begin{aligned} f(v_p) &= p(v_p)\exp\left(-\ln 2\frac{\Gamma_0}{\Gamma_c}\exp\left\{-\frac{1}{k_B T}\left[E_a(v_c) + \left.\frac{\partial E_a}{\partial v}\right|_{v_c}\delta v\right]\sum_{1}^{N}\exp\left[\frac{-2}{\ln 2}\frac{n\,\delta v_d}{\Delta v_c}\right]\right\}\right) \\ &= p(v_p)\exp\left\{-\ln 2\exp\left(\frac{2}{\ln 2}\frac{\delta v}{\Delta v_c}\right) \times \sum_{1}^{N}\exp\left(\frac{-2}{\ln 2}\frac{n\,\delta v_d}{\Delta v_c}\right)\right\} \\ &= [1 - \exp\{-\ln 2\, e^z\}]\exp\left\{-\ln 2\, e^z \sum_{1}^{N} e^{-n z_d}\right\}. \end{aligned} \tag{24}$$

We have introduced $z = 2(v_p - v_c)/(\Delta v_c \ln 2)$ and $z_d = 2\,\delta v_d/(\Delta v_c \ln 2)$ to simplify notations in the expressions of the probability that a (single) phase slip takes place during a given half cycle with peak amplitude v_p, Eq. (23), and of the probability distribution that a (single) phase slip takes place during the half cycle with velocity v_p after a sequence of N half cycles starting from a resonance amplitude at which $p(v_p)$ is low with an increase in peak amplitude δv_d from one half cycle to the next, Eq. (24).

The cumulative probability P corresponding to the latter case is given by

$$P = \int_{-\infty}^{z} f\,dz/\mathcal{N} = \int_{-\infty}^{z}[1 - \exp\{-\ln 2\, e^z\}]\exp\{-\mu e^z\}\,dz/\mathcal{N}, \tag{25}$$

the normalization constant being $\mathcal{N} = \int_{-\infty}^{\infty} f\,dz$ and

$$\mu = \ln 2\, e^{-z_d}\frac{1 - \exp(-N z_d)}{1 - \exp(-z_d)}.$$

If the slip probability at the beginning of the N-half-cycle sequence, $p(v_p - N\,\delta v_d)$, is low enough, N can be arbitrarily increased in Eq. (21) and P becomes independent of N. In the large N limit, $\mathcal{N}$ can be shown to reduce to z_d and P is expressed in terms of the exponential-integral function[79]

$$P = 1 - [E_1(\mu x + x\ln 2) - E_1(\mu x)]/z_d \tag{26}$$

with $x = e^{-z}$.

The apparent, or average, critical velocity at a given excitation level is then obtained as the statistical mean value of v:

$$\begin{aligned} v_a &= \int_0^{\infty} v\, f\,dv/z_d = v_c + \frac{\ln 2}{2}\frac{\Delta v_c}{z_d} \\ &\quad \times \int_{-\infty}^{\infty} z[1 - \exp\{-\ln 2\, e^z\}]\exp\{-\mu e^z\}\,dz. \end{aligned} \tag{27}$$

The integral in Eq. (27) again involves exponential-integral functions and yields

$$v_a = v_c - \frac{\ln 2}{2}\Delta v_c\left[\mathcal{C} + \ln(\ln 2) + \ln\frac{e^{-z_d/2}}{1 - e^{-z_d}}\right]. \tag{28}$$

Euler's constant $\mathcal{C} = 0.577\,21\ldots$ and $z_d = 2\,\delta v_d/(\Delta v_c \ln 2)$ as before. Equation (28) describes the effect of the drive level on the apparent critical velocity in ac experiments, i.e., the mean peak amplitude at which slips occur is observed to rise when driving the hydromechanical resonator harder on resonance (see Ref. 68 for an example).

The mean-square deviation of the apparent critical velocity, Δv_a, is similarly defined in terms of the probability distribution given by Eq. (26) as

$$(\Delta v_a)^2 = \int_0^{\infty}(v - v_a)^2 f\,dv/z_d = \overline{(\delta v^2)} - (v_a - v_c)^2.$$

The mean-square deviation $\overline{(\delta v^2)}$ of $\delta v = v_p - v_c$ is given by the following integral,

$$\overline{(\delta v^2)} = \frac{1}{z_d}\left(\frac{\ln 2}{2}\Delta v_c\right)^2 \int_{-\infty}^{\infty} z^2 f\,dz,$$

which can be evaluated by differentiation with respect to μ under the integral sign and subsequent integrations. A somewhat laborious calculation leads to the simple result

$$(\Delta v_a)^2=\frac{\pi^2}{6}\left(\frac{\ln 2}{2}\Delta v_c\right)^2+\frac{1}{12}(\delta v_d)^2. \tag{29}$$

In the limit $\delta v_d \ll \Delta v_c$, the critical width is simply proportional to the root-mean-square (rms) deviation of the apparent critical velocity. The measurement of Δv_a gives Δv_c by Eq. (29) and Γ_c by Eqs. (17) and (19); that of v_a yields the true critical velocity v_c by Eq. (28). Hence, the knowledge of v_a and Δv_a gives access to the nucleation rate at velocity v_c.

In the same limit $z_d \leqslant 1$, P, expressed in terms of transcendental functions by Eq. (26), can be put under a simpler and more transparent form as follows. Consider integral (25) for P and restrict the analysis to $z=2(v_p-v_c)/\Delta v_c \ln 2 \leqslant 0$. In this case, e^z is small and Eq. (25) can be readily integrated as follows:

$$\begin{aligned}P &\simeq \int_{-\infty}^{z}[1-\exp\{-\ln 2\, e^{z'}\}]\exp\{-\ln 2\, e^{z'}/z_d\}\frac{dz'}{z_d}\\ &\simeq \int_{-\infty}^{z}\frac{\ln 2}{z_d}e^{z'}\exp\left\{-\frac{\ln 2}{z_d}e^{z'}\right\}dz'\\ &=1-\exp\{-\ln 2\,\exp(z-\ln z_d)\}.\end{aligned} \tag{30}$$

Expressions (23) for p and (30) for P are strikingly similar. For small to moderate drive levels ($z_d \leqslant 1$) (which implies that phase slips occur at low resonance amplitudes so that v_p remains below v_c on average) Eq. (23) even reduces exactly to Eq. (30) with a velocity at $P=1/2$, the median velocity, shifted downward from v_c by an amount proportional to $\ln z_d$:

$$v_{1/2}=v_c+\frac{\ln 2}{2}\Delta v_c \ln\left(\frac{2}{\ln 2}\frac{\delta v_d}{\Delta v_c}\right). \tag{31}$$

The slope of P at $P=1/2$ is, in this parameter range, equal to that of $p(v_p)$ at v_c. The critical width Δv_c of the transition can be obtained indifferently from both probability curves but p involves no correction for the drive.

IV. THE EXPERIMENTAL RESULTS

The experiments on ultrapure ^{4}He, the analysis of which constitutes the main body of this paper, were carried out in 1992–1993 and are reported in Refs. 4 and 10. Since then, a number of improvements have been implemented in our software program for peak amplitude chart analysis, which we summarize below. To illustrate the various statistical approaches described in the previous section, we treat as an example the high quality data obtained on interferometric measurements of the rotation of the Earth.[70,71,80] We next turn to the reanalysis of the original data of 1992–1993 with the implementation of the direct determination of the slip nucleation rate.

A. Improvements in the raw data analysis procedure: The 100-ppb sample

The peak amplitude chart analysis has been improved in two ways. First, in the course of detailed studies of multiple slips,[69,81] and, in particular, after having realized that there were two kinds of large slips with very different properties, we were led to develop better recognition schemes for these slips which give a more precise evaluation of the slip multiplicity.

Second, for high-resolution superfluid interferometry measurements of the rotation of the Earth,[70,71,80] we have further improved the raw data processing to achieve a more accurate determination of the circulation bias κ_b. In particular, as reported in Ref. 70, it proved necessary to take into account a small statistical unbalance induced by the trapped circulation in the loop which increases the probability of slips along the trapped flow direction and decreases the overall time spent by the system in the corresponding state. This asymmetry built into the data is corrected by constructing two histograms, one for slip number in velocity bins, the other for the total time spent by the resonator in each of these velocity bins: the rate $\Gamma(v)$ is, according to its definition, the ratio of the number of slips at velocity v to the total lapse of time during which the system has been found at that velocity. Since time is a continuous quantity expressed in seconds, its graph as a function of velocity does not constitute, strictly speaking, a histogram. The total time spent by the system in each velocity bin is computed using the fact that the resonator motion is very nearly purely sinusoidal.[69]

A further refinement is needed to achieve maximum accuracy: a slip does not necessarily nucleate sharply at the peak velocity and the (small) difference between the actual slip velocity and the peak velocity must be taken into account. In the raw data acquisition, the collected information is the peak amplitude of the resonator motion at each half cycle, and for large slips, the delay between the peak and the slip times. The correction between actual and peak velocity can be computed from this delay. For low-multiplicity slips, this delay is too small to be resolved experimentally and the small correction to the slip velocity cannot be made.

To work around this difficulty, we use the knowledge of the statistical properties of the slip distribution that has been gained at this stage of the data analysis. The probability dp that a slip occurs between t and $t+dt$ is given by Eq. (12). If it is known for certain that a slip has taken place during the half cycle t_i to t_f for which the slip probability $p(v_p)$ is given by Eq. (15), then the probability density $d\bar{p}$ that this certain event has occurred between t ($t_i<t<t_f$) and $t+dt$ is $d\bar{p}=dp(t)/p(v_p)$. This density can be integrated by expanding $E_a(t)$ about the peak of the half cycle assumed at $t=0$, $E_a(t)=E_a(v_p)+\frac{1}{2}\partial E_a/\partial v|_{v_p}\omega^2 t^2$, with the following result:

$$\bar{p}=1-\exp\left\{-\frac{1}{2}Y(v_p)[1+\mathrm{erf}(\bar{\omega}t)]\right\}, \tag{32}$$

in which $\bar{\omega}=[-(v_p/2k_BT)(\partial E_a/\partial v)|_{v_p}]^{1/2}\omega$, and

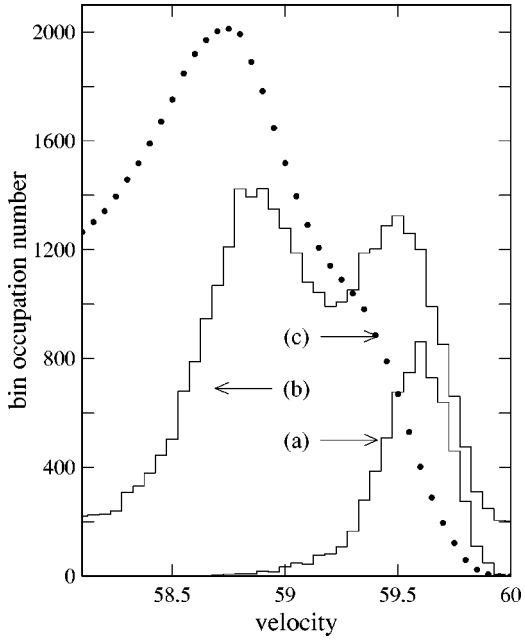

FIG. 3. Histograms for the 100 ppb sample of (a) the number of slips in velocity bins of size 0.05 winding number, (b) the number of half cycles with peak amplitudes in the same velocity bins (offset upward by 200 units for clarity), and (c) the total time during which the flow velocity in the aperture was found in the same bins, with one vertical unit corresponding to 3 ms. Velocities are expressed as winding numbers of the quantum phase difference as given by Eq. (11). The resonator frequency is 9.23 Hz, and the ratio R, 1.025. Here, the slips are assumed to have occurred at the peak velocity. Similar histograms can be constructed with the slip velocities spread around the peak in a probabilistic manner as described in the text.

$$Y(v_p) = -\ln\{1-p(v_p)\} = \ln 2 \exp\left\{\frac{2}{\ln 2}\frac{v_p - v_c}{\Delta v_c}\right\}.$$

The probability distribution of the slip velocity in the half cycle can thus be evaluated to fair accuracy knowing v_a and Δv_a. Then, the slip velocities of a given data set are spread at random according to Eq. (32) in each half cycle with a slip. This procedure mimics the actual spread in velocity of the slips about the peak velocity and yields a slip velocity histogram closer to reality. The validity of this ''self-tailing'' procedure has been checked by direct numerical simulations.[70]

Examples of histograms obtained in this way for the superfluid interferometry experiments reported in Refs. 70,71 and 80 are given in Fig. 3. These experiments were carried out at a temperature of 12 mK at 0.6 bar on a ^{4}He sample containing 100 ppb of ^{3}He impurities. The statistical width Δv_c is significantly reduced with respect to that in ultrapure ^{4}He, which increases the resolution on the phase bias. The drive amplitude was fairly large ($\delta v_d = 0.247$) so as to obtain many slips per data record and to increase the size of the statistical sample.

The probability of a slip during a given half cycle of the resonance peaking at v_p, $p(v_p)$, is obtained by dividing the bin to bin histogram (a) in Fig. 3 by the histogram (b). The cumulative probability that a slip has occurred at or before v_p, $P(v_p)$, is obtained by integrating the histogram (a) in Fig. 3 and normalizing by the total number of slips in the statistical sample. Slips which immediately follow another slip have not been retained in the analysis since they may correspond to a state of the resonator slightly off steady state.

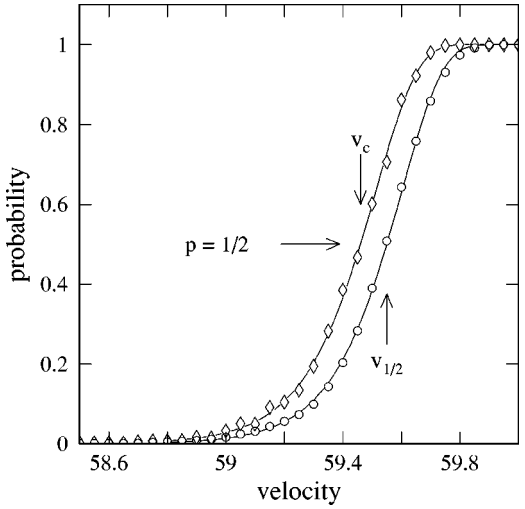

FIG. 4. Probabilities p ($\diamond$) and P ($\bigcirc$), obtained from the histograms in Fig. 3 as explained in the text. The plain curves are nonlinear least-squares fits to the analytical form (23) or (30).

Probability distributions p and P are shown in Fig. 4.[82] According to Eqs. (23) and (30), both distributions display the same slope at probability 1/2 although the condition that $z_d \lesssim 1$ is not quite fulfilled ($z_d = 1.89$); the shift between v_c and $v_{1/2}$ in Fig. 4 is 0.090; that predicted by Eq. (31) is 0.083. The value of v_c obtained from $p = 1/2$ is 59.460 in a winding number.

The resulting nucleation rate obtained by dividing the slip number histogram [Fig. 3(a)] by the residence time in each velocity bin [Fig. 3(c)] is shown in Fig. 5. As seen in Fig. 5, taking into account the fact that slip velocities are scattered about v_p with the help of Eq. (32) introduces significant corrections at small residence times (large velocities).

The quantity $\ln\Gamma$ depends linearly on v over the restricted range of values scanned by the natural spread of the nucleation velocity: $\ln\Gamma = Av + B$. From the slope A of $\ln\Gamma$ as a function of v and expression (14), we deduce that

$$A = -\frac{1}{k_B T}\left.\frac{\partial E_a}{\partial v}\right|_{T, v\sim v_c} \simeq \frac{2}{(\ln 2)\Delta v_c} \qquad (33)$$

in inverse winding number. The approximate equality on the rhs results from Eq. (19). The fit in Fig. 5 yields $A = 7.086 \pm 0.11$ (the statistical spread being taken into account). This quantity is also obtained from the nonlinear fits shown in Fig. 4 which yield 6.98 ± 0.08 for p (and 7.149 ± 0.06 for P, which differs slightly from the value for p since $z_d \gtrsim 1$). These values differ by less than 2%: the statistical width of the critical velocity transition is fairly accurately determined from these high-precision data.

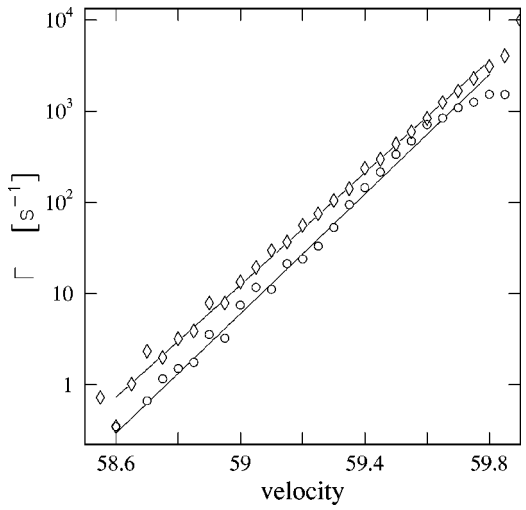

FIG. 5. Nucleation rate in inverse seconds on a logarithmic scale vs velocity, obtained from the histograms in Fig. 3 with slip velocities assumed at the peak velocity v_p (○) and when taking the statistical spread about v_p into account with the help of Eq. (32) (◇). The plain curves are linear fits to the data.

The offset B of the linear fit to $\ln\Gamma$ yields the value of the critical velocity with the help of Eq. (17) which can be rewritten

$$B = -A\,v_c + \ln[(\ln 2)\,\omega\sqrt{Av_c/2\pi}]. \tag{34}$$

Solving Eq. (34) for v_c with $B=-416$ yields $v_c=59.47$, a value very close to that obtained from p, 59.46, as quoted above. The agreement is not surprising since the two methods of analysis are basically equivalent, except that the nucleation rate analysis yields directly an accurate value of $\ln\Gamma_c = Av_c + B$.

Finally, the measured values of v_a (59.736) and Δv_a (0.182), lead, with the help of Eqs. (28) and (29), to $v_c = 59.669$ and $A = 2/\ln(2)\Delta v_c = 7.66$, in fair but not excellent agreement with the above determinations. It must be noted, however, that the assumptions made in deriving Eq. (21) are not fully justified since slips occur frequently in these data.

From these tests of the data analysis procedures on the high quality data obtained with the 100-ppb sample, we conclude that, although the various data analysis methods all provide the same information, the direct determination of Γ is more precise and less biased. We now apply the same statistical analysis to the ultrapure sample case.

B. Ultrapure ^{4}He

Two different samples of ultrapure ^{4}He were studied at a pressure close to SVP from about 18 mK to 500 mK. The experimental data were of a lesser quality than those for the 100-ppb sample discussed in the previous section, in particular, because the data records were shorter and slip statistics poorer. A complete reanalysis of the original data implementing the various improvements in the data analysis software discussed above was still deemed in order; it is given below.

The results from the two methods of analysis, from the average values and direct from the nucleation rate, are collected in Table I. The mean value v_a and the root-mean-square deviation from the mean Δv_a are computed over a data sample of several hundreds of slips at a given temperature. The first three columns of Table I give T, v_a, and Δv_a. The real critical velocity v_{c-a} and the transition width Δv_{c-a} are computed with the help of Eqs. (28) and (29) knowing that the change in the resonance amplitude forms one half cycle to the next δv_d caused by the drive. These quantities are given in columns 4–6, as well as Γ_{c-a}, computed from Eq. (17) and the approximate relation (19) given in column 7.

The determination of the nucleation rate as a function of v follows that outlined in Sec. IV A for the 100-ppb sample. It yields in turn the two parameters A and B such that $Av+B = \ln\Gamma(v)$. These quantities are given in columns 8 and 9 of Table I, A being put under the form $\Delta v_{c-n} = 2/(A\ln 2)$ for comparison with Δv_{c-a}. The critical velocity derived from the nucleation rate analysis v_{c-n} is computed from A and B with Eq. (34), and the logarithm of the nucleation rate at v_c, $\ln\Gamma_{c-n}$, from Av_c+B. These quantities are given in columns 10 and 11, respectively.

As an illustration, $\ln\Gamma$ for the data corresponding to the first row of Table I (at $T=17.70$ mK) is plotted vs v in Fig. 6 as well as the straight-line fit which yields parameters A and B. The probability distributions p and P are plotted for the same temperature in Fig. 7, together with the nonlinear fit curves adjusted to Eqs. (23) and (30). The values derived from these plots for critical velocities corresponding to v_a, $v_{1/2}$ and $v_{p=1/2}=v_c$ calculated with Eqs. (28) and (31) are 40.564, 40.517, and 40.660, respectively. The quantity Δv_c is less well determined. It is found to be 0.316 and 0.355 from p and P, respectively, and 0.338 and 0.399 from v_a and A.

The rate Γ in Fig. 6 is less affected by noise and poor statistics than is the probability p in Fig. 7. In view of the scatter on p and P in Fig. 7, the agreement on v_c and Δv_c between the various determinations appears satisfactory, but the remaining differences stress the importance of using the most direct nucleation rate determination in a systematic manner: we keep in the following the transition widths obtained from the nucleation rate, which, furthermore, represent $\partial E_a/\partial v|_{T,v\simeq v_c}$ without approximation.

The determination of critical velocity which shows less scatter is v_{c-a}, and this is also the most direct. The velocities v_{c-a} and v_{c-n}, obtained from Eq. (34), compare well with one another, which constitutes a consistency check on the data. They are plotted in terms of T in Fig. 8: the thermal regime where v_c decreases in a near-linear way with T and the low temperature plateau, where it stays nearly constant, are well delineated with a sharp transition between the two.

The transition width Δv_{c-n}, plotted in terms of T in Fig. 9, also exhibits a well-marked transition between thermal and quantum regimes. The dotted line in Fig. 9 represents the width as calculated from the final values of this analysis, collected in Table II (see the discussion in Sec. V C).

The errors on v_{c-n} are correlated with those on A and B, and those on $\ln\Gamma_c = Av_c + B$. For this reason, v_{c-n} is retained instead of v_{c-a} in the analysis of the following section

TABLE I. Experimental data.

T (mK)	v_a	Δv_a	δv_d	Δv_{c-a}	v_{c-a}	$\ln(\Gamma_{c-a})$	Δv_{c-n}	B	v_{c-n}	$\ln(\Gamma_{c-n})$
17.70	40.440	0.151	0.0502	0.338	40.564	5.65	0.399	−288.21	40.660	5.91
17.80	40.448	0.143	0.0507	0.320	40.558	5.68	0.400	−287.33	40.663	5.92
18.60	40.382	0.163	0.0508	0.365	40.524	5.61	0.419	−274.03	40.610	5.89
20.00	40.441	0.150	0.0506	0.336	40.563	5.65	0.409	−281.32	40.665	5.90
20.30	40.338	0.150	0.0498	0.336	40.460	5.65	0.423	−271.06	40.562	5.89
28.80	40.326	0.165	0.0501	0.370	40.471	5.60	0.457	−250.18	40.578	5.85
28.85	40.353	0.157	0.0504	0.352	40.487	5.63	0.405	−283.08	40.570	5.90
56.80	40.483	0.154	0.0500	0.345	40.613	5.63	0.416	−276.18	40.709	5.89
58.30	40.339	0.168	0.0501	0.377	40.491	5.59	0.440	−260.39	40.581	5.86
100.70	40.277	0.224	0.0494	0.503	40.533	5.45	0.468	−244.31	40.549	5.83
103.20	40.455	0.163	0.0495	0.365	40.600	5.61	0.440	−261.12	40.698	5.86
103.21	40.346	0.158	0.0480	0.354	40.487	5.62	0.414	−277.12	40.573	5.89
127.30	39.885	0.219	0.0448	0.492	40.150	5.45	0.461	−245.41	40.137	5.83
130.00	40.246	0.247	0.0573	0.554	40.518	5.40	0.582	−195.72	40.627	5.72
150.00	39.304	0.254	0.0370	0.571	39.678	5.37	0.519	−214.55	39.627	5.77
161.50	39.428	0.280	0.0549	0.629	39.773	5.33	0.620	−179.62	39.828	5.68
177.00	38.951	0.280	0.0420	0.629	39.356	5.32	0.592	−185.91	39.328	5.70
188.70	38.614	0.309	0.0507	0.694	39.039	5.27	0.638	−170.89	39.035	5.66
201.50	38.244	0.287	0.0381	0.645	38.687	5.30	0.640	−168.80	38.676	5.65
215.00	38.248	0.319	0.0452	0.717	38.725	5.25	0.687	−157.05	38.712	5.62
242.20	37.479	0.338	0.0415	0.760	38.021	5.21	0.737	−143.20	37.979	5.57
249.00	37.068	0.306	0.0290	0.688	37.619	5.26	0.689	−151.63	37.547	5.60
300.50	35.576	0.329	0.0060	0.740	36.572	5.21	0.781	−128.38	36.275	5.51
358.60	35.044	0.348	0.0347	0.783	35.657	5.16	0.958	−101.96	35.641	5.41
419.00	34.276	0.342	0.0659	0.768	34.704	5.16	0.943	−100.98	34.747	5.40

where the activation energy $E_a(v)$ and the barrier energy $E_b(v)$ after due allowance to the quantum and the depopulation corrections are extracted from the nucleation rate data.

V. DISCUSSION

The nucleation rate shows two regimes in terms of temperature. Below ~0.12 K, it levels off and reaches a plateau. Above ~0.12 K, it exhibits a marked dependence on temperature. The high-temperature dependence and that of v_c constitute direct evidence for thermally assisted nucleation, as discussed in Ref. 78. It was once believed that only large vortices were involved in the critical velocity problem; large

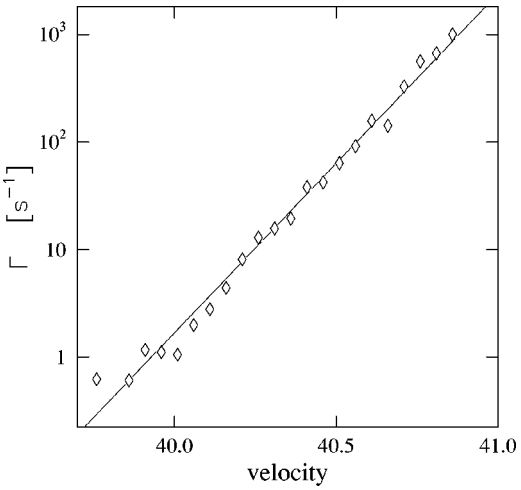

FIG. 6. Nucleation rate Γ expressed in s^{-1} vs slip velocity in winding number in ultrapure ^{4}He at 17.70 mK on a semilogarithmic scale. The plain line represents a linear fit to the data which yields the quantities Δv_{c-n} and B given in Table I.

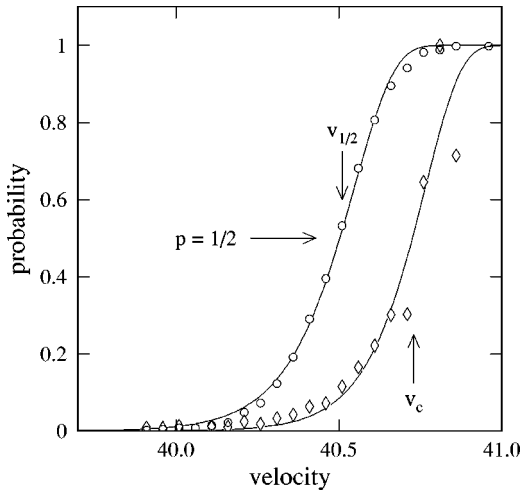

FIG. 7. Probabilities p (◇) and P (○) vs slip velocity in winding number for the ultrapure sample at 17.70 mK. The plain curves are nonlinear least-squares fits to the analytical forms (23) and (30) which contain two unknown parameters, v_c and Δv_c. In contrast to Fig. 4, $v_{1/2}$ is smaller than v_c because δv_d is small, the shift given by Eq. (31) being −0.140.

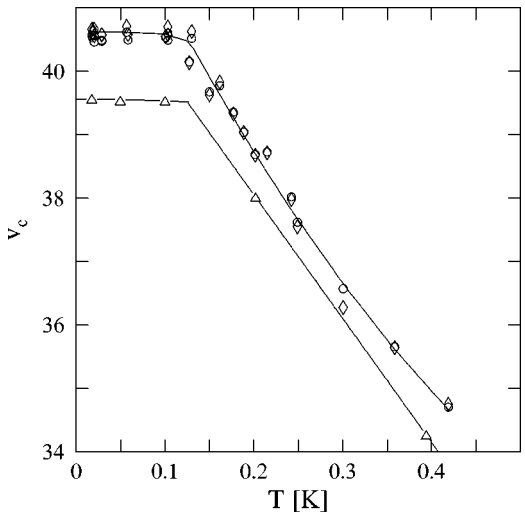

FIG. 8. The critical velocity v_c, in winding number, vs T in K for the two ultrapure samples: v_{c-a}, from column 6 in Table I (○); v_{c-n}, from column 10 (◇); and v_{c-n} for the 0.9-ppb ^{3}He in the ^{4}He sample (△). The plain lines are linear fits to the data for (△), a cubic spline smoothed imposing a rms deviation of 0.12 for (◇), yielding the values of column 2 in Table II.

objects usually involve large energies for their formation, and hence, are unlikely to be thermally nucleated. Such is not the case in small pores,[83] for ion propagation,[84] and for microaperture flows, where nanometer-size vortices are formed, as is now well established.[55,76]

That the occurrence of a plateau at low temperature implies quantum tunneling is more open to discussion.[17,18,51] There are three main courses for disbelief, (i) that the experimental evidence for intrinsic saturation—the plateau of v_c—is not iron-clad, (ii) that no proof is given that the plateau, if intrinsic, is caused by the onset of quantum tunneling and not by some other mechanism, and, finally, (iii) that a process involving a large number of particles in strong coupling with their environment has no chance to exhibit collective quantum motion.

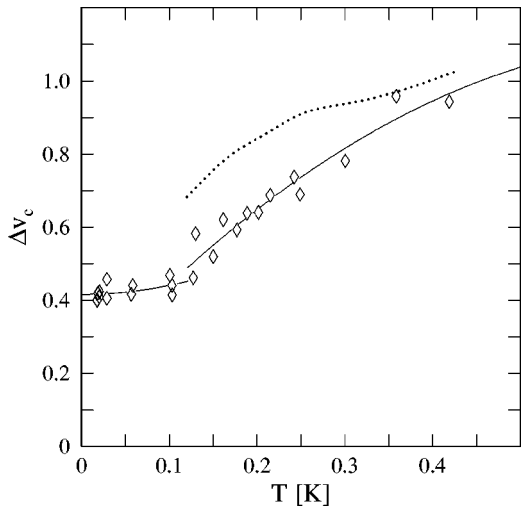

FIG. 9. The critical width Δv_c, in winding number, vs T in K: from column 8 in Table I (◇); for the 0.9-ppb ^{3}He in the ^{4}He sample (△). The plain lines are parabolic fits to the (◇) data to guide the eye. The dotted curve is the (smoothed) width computed from the values for Table II, as a closure for the numerical analysis.

TABLE II. Smoothed v_c vs temperature, its derivative with respect to T, the chosen values of α and the computed quantum corrections, depopulation factor, and energy barrier. The values of ω_0 are derived from Eq. (5) with $T_0 = 0.144$ K.

T (mK)	v_c	dv_c/dT	α	$\ln f_q$	$\ln \Upsilon$	E_b (K)
17.70	40.6235	−0.07	0			2.795
17.80	40.6235	−0.08	0			2.795
18.60	40.6234	−0.14	0			2.796
20.00	40.6232	−0.13	0			2.796
20.30	40.6232	−0.13	0			2.796
28.80	40.6217	−0.23	0			2.797
28.85	40.6217	−0.23	0			2.797
56.80	40.6125	−0.41	0.001			2.802
58.30	40.5885	−0.42	0.001			2.802
100.70	40.5664	−8.17	0.007			2.816
103.20	40.4715	−49.81	0.008			2.829
103.21	40.4715	−49.96	0.008			2.829
127.30	40.4035	−23.04	0.013	5.437	0	2.884
130.00	40.4035	−25.13	0.014	5.125	0	2.924
150.00	39.9082	−24.40	0.019	3.589	−0.015	3.214
161.50	39.6300	−23.98	0.022	3.099	−0.033	3.380
177.00	39.2626	−23.42	0.026	2.344	−0.042	3.605
188.70	38.9911	−22.99	0.030	2.000	−0.042	3.780
201.50	38.6998	−22.52	0.033	1.716	−0.039	3.976
215.00	38.3991	−22.03	0.037	1.484	−0.034	4.191
242.20	37.8133	−21.04	0.045	1.147	−0.025	4.642
249.00	37.6711	−20.79	0.047	1.081	−0.023	4.758
300.50	36.6487	−18.91	0.063	0.731	−0.012	5.670
358.60	35.6114	−16.79	0.081	0.509	−0.005	6.712
419.00	34.6635	−14.59	0.100	0.371	−0.003	7.725

Let us deal first with experimental problems. It is a fact that the occurrence of such a saturation effect at low temperature may have many causes, as debated in the literature, e.g., in Refs. 85–87, for systems other than helium. In the present case, the plateau of v_c has been observed at a reproducible crossover temperature in a number of different runs with different samples, two of ultrapure ^{4}He at low pressure as reported here, a number of impure ^{4}He samples at different pressures, and in a study of a series of ^{3}He-^{4}He mixtures at different concentrations in the few parts per billion range.[75] This last work also shows most directly that the temperature of the resonator follows that of the thermometers since the effect of ^{3}He impurities can be tracked down to the bottom temperature of the refrigerator.

Mechanical vibrations are a serious issue in these experiments, especially for the measurement of the critical transition width Δv_c. A number of steps have been taken to reduce the background mechanical noise, which can trigger critical velocity events in a way independent of temperature. It has been demonstrated that the level of residual spurious rotations in the setup at Saclay amounts to less than 7×10^{-8}(rad/s)/$\sqrt{\text{Hz}}$,[88] several orders of magnitude below the

noise on v_c and Δv_c reported here, and down by even more below the level necessary to cause a plateaulike saturation.

A leveling off of v_c has also been observed in impure ^{4}He by Davis *et al.*[49] who also interpreted their observation as evidence for quantum tunneling. Their work can be seen as a qualitative confirmation of the present work, but these authors found the onset of the plateau at a temperature of $\sim$180 mK instead of 120 mK as reported here. It is not known whether this difference represents an intrinsic feature of the aperture or an extrinsic feature of the measuring apparatus.

Having established that the plateau occurrence in our experiments is not due to extraneous effects, we now address the second concern mentioned above, namely, that it would signal not the takeover of quantum tunneling but rather a bifurcation to some other, non-quantum, mechanism, a hydrodynamical instability fostered by the flow such as the formation of Kadomtsev-Petviashvili solitons,[89] bubbles,[90] or vortex mills.[91] We argue, as in Ref. 55, that since the variations of both v_c and Δv_c are continuous, though rapid, around T_0, the energy barrier experiences no abrupt change, and that, in all likelihood, the mechanism for vortex formation, or phase-slip appearance, remains the same. The determination of E_b, which follows, establishes this last point in a quantitative manner.

The third of the concerns expressed above is of a more conceptual nature. The work on electrodynamic Josephson devices referred to in the Introduction yields clear experimental evidence of the existence of quantum behavior in macroscopic variables. For hydrodynamical objects that possess topological stability such as vortices in helium, such a concern should be considered in light of the internal consistency of the analysis of the experimental data in terms of quantum tunneling, to which we now turn.

A. The Arrhenius plot at low *T*

The nucleation rate becomes very nearly temperature independent below $\sim$100 mK. The crossover between this low-temperature (LT) quantum-tunneling regime and thermal activation at higher temperature takes place slightly above the knee in the v_c vs T curve, which lies at 120 mK. The precise determination of T_0, which turns out to be 0.144 K, is tackled below.

In order to analyze in greater detail the raw data of Table I, we proceed with a number of steps. As a first step, we construct an Arrhenius plot by plotting the logarithm of the nucleation rate $\ln\Gamma(v)$ as a function of $1/T$ holding the velocity v equal to its $T=0$ value, v_q (obtained by extrapolation of the data in Fig. 8). On the LT plateau, $\ln\Gamma(v_q) = \ln\Gamma_c + A(v_q - v_c)$ since the correction is small.

The LT part of the curve of $\ln\Gamma(v_q)$ is extremely flat, from which we conclude with the help of Eq. (7) that damping at LT must be very small. A fit to Eq. (7) yields $\ln\Gamma = 5.900\ (\pm 0.007) - 0.48(\pm 2.16)T^2$, Γ being expressed in s^{-1}. We note that the coefficient of T^2 is negative while, from Eq. (7), we would have expected it to be positive.

In fact, as seen in Fig. 10, $\ln\Gamma(v_q)$ exhibits a shallow trough around 0.1 K where it lies below the logarithm of the rate calculated at zero damping with the help of the numerical tables of Grabert *et al.*[56] The values of $\ln\Gamma(v_q)$ obtained from the raw data of Table I, shown as ($*$) in the main frame of Fig. 10, lie significantly lower than the computed values around 0.1 K. It should be noted that $\ln\Gamma(v_q)$ shows more scatter than $\ln\Gamma_c$. This simply reflects the noise on $v_c - v_q$. The inset displays the trough more clearly, the scatter on $\ln\Gamma(v_q)$, shown by (■), being reduced by using smoothed values for $v_c(T)$ (see Table II) in the correction from $\ln\Gamma(v_c)$ to $\ln\Gamma(v_q)$.

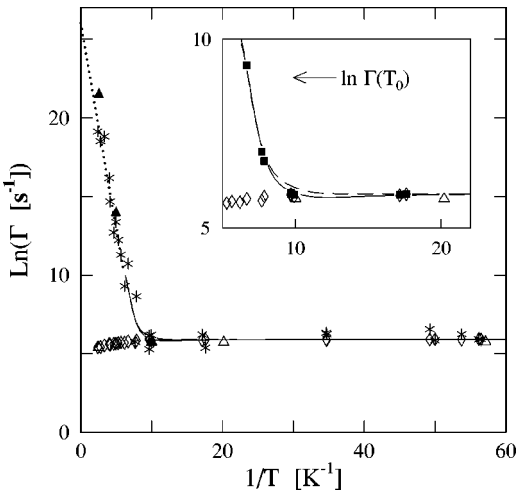

FIG. 10. $\ln\Gamma(v)$ vs $1/T$, Γ being expressed in s^{-1} and T in K: $\ln\Gamma_c$ from Table I (◇); $\ln\Gamma(v_q)$ corrected for the change of the velocity with T as explained in the text ($*$). The raw data (△) and the corrected values (▲) from the run with the second sample of ultrapure ^{4}He agree very well with those of Table I. In the inset, $\ln\Gamma(v_q)$ (■) has been obtained with the smoothed values of v_c of Table II. The curves represent the calculated values of $\ln\Gamma(v_q)$ with $\alpha=0$ (dashed line) or varying with T (plain line) as explained in the text. The dotted curve is the extrapolation to $1/T=0$ of a linear fit to the high-temperature portion of the data.

Thus, the observed crossover between the thermal and the quantum regimes appears even sharper than that predicted for zero damping. This feature also shows in the abruptness of the break of $v_c(T)$ around T_0. It can be accounted for by a rapid variation of α with temperature close to 0.1 K from practically zero at $T < T_0/2$ to 0.01 at $\sim$0.1 K, and 0.02 at $\sim$0.15 K.

A least-squares reduction of the raw $\ln\Gamma(v_q)$ to the theoretical curves adjusting E_b at $T=0$, $\alpha(T)$, as expressed analytically as described below, and T_0 yields the plain curve shown in Fig. 10. The energy barrier $E_b(T=0)$ is accurately determined by the low-temperature extrapolation of $\ln\Gamma(v_q)$. The crossover temperature T_0, 0.144 K, is also well-pinned down by the fitting procedure. The best fitting $\alpha(T)$, $0.06/(\exp\{0.23/T\}-1)$, results mainly from the dip in $\ln\Gamma(v_q)$ close to 0.1 K and is more loosely fixed. The resulting fit to the raw $\ln\Gamma(v_q)$ is also shown in the inset of Fig. 10; it agrees well with the values of $\ln\Gamma(v_q)$ computed from $\ln\Gamma(v_c)$ using *smoothed* values for v_c. It thus turns out that damping in vortex nucleation can be fairly well estimated from these experiments, which is possible only because the

quantum-tunneling rate is suppressed exponentially by the coupling to the environmental bath.[24]

B. The Arrhenius plot at high T

As T increases above T_0 and v_c drops below v_q, the variation of A with v must be taken into account. At this first stage of the analysis, we do not retain the difference between E_a and E_b and we assume that ω_0 is a constant and that E_b is independent of T. With these assumptions, which are re-examined in the following sections, we simply have $\ln\Gamma(v,T)=\ln(\omega_0/2\pi)-E_b(v)/k_BT$ as given by the Arrhenius law, Eq. (1). We then use the experimentally determined $A=\partial\ln\Gamma/\partial v|_T$ through the relation

$$\left.\frac{\partial E_a}{\partial v}\right|_T=\frac{dE_b}{dv}=-k_BTA, \tag{35}$$

and obtain high-temperature part of the Arrhenius plot in Fig. 10 by numerical integration of Eq. (35):

$$\ln\Gamma(v_q,T)=\ln\Gamma_c(T)-(1/k_BT)\int_{v_c(T)}^{v_q}\frac{dE_b}{dv}dv.$$

As seen in Fig. 10, the outcome for $\ln\Gamma(v_q,T)$ depends linearly on $1/T$ with a slope equal to -2.62 in kelvin, and an intercept at $1/T=0$ of 26.0. The latter value is quite comparable to $\ln\omega_0/2\pi\simeq\ln k_BT_0/\hbar=23.66$, the former to $-E_b(v_q)$, which is of the order of -2.8 K as derived below. A precise agreement between the LT determination of E_b and the high-temperature extrapolation cannot be expected to hold at this first-order step of the analysis but it is already clear that the LT plateau and the thermally activated region can be accounted for by a single nucleation mechanism and a smooth dependence of E_b upon v. Invoking different vortex formation processes for each regime would, in all likelihood, lead to quite different values of E_b and dE_b/dv.

C. Energy barrier vs velocity

We now build on the above determination of $\omega_0(=\omega_b)$, still assumed constant, and proceed to derive E_b at $v_c(T)$ from the complete expression for the rate, Eq. (9), the logarithm of which reads

$$\ln\Gamma(T,v)=\ln\left\{\frac{\omega_0}{2\pi}[\sqrt{1+\alpha^2}-\alpha]f_q\Upsilon\right\}-\frac{E_b}{k_BT}. \tag{36}$$

To evaluate Eq. (36) and to determine the quantum and depopulation corrections f_q and Υ, given by Eqs. (4), (8), and (10), we have to assign values to the damping coefficient α for which we have obtained estimates below T_0 only in the previous paragraph. To obtain an evaluation of α in the thermal regime, we consider the derivative of $\ln\Gamma$ with respect to T, which reads

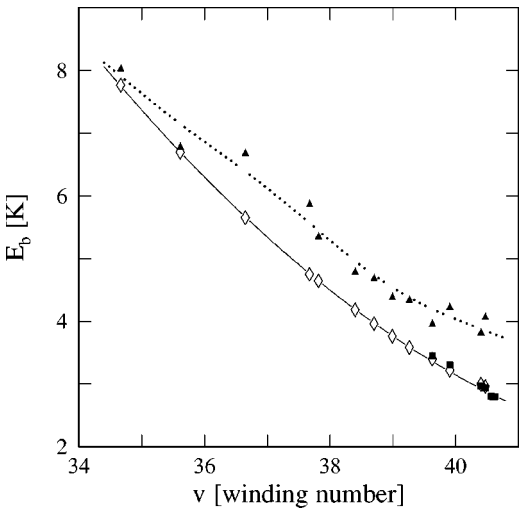

FIG. 11. The barrier energy E_b in kelvin vs v, the velocity in the aperture expressed in winding number obtained from the LT data transformed using the tables in Ref. 56 (■); from Eq. (36) (◇); from Eq. (37) assuming $\partial E_b/\partial T|_v=0$ (▲). The plain curve is a second-order polynomial fit, and the dotted line is a guide for the eye obtained from a cubic spline smoothing routine imposing a rms deviation of 0.2.

$$\left.\frac{\partial\ln\Gamma(T,v)}{\partial T}\right|_v=-\frac{1}{(1+\alpha^2)^{1/2}}\left.\frac{\partial\alpha}{\partial T}\right|_v+\left.\frac{\partial\ln f_q\Upsilon}{\partial T}\right|_v-\frac{1}{k_BT}\left.\frac{\partial E_b}{\partial T}\right|_v+\frac{1}{T}\frac{E_b}{k_BT}. \tag{37}$$

Equation (37) gives, assuming that $\alpha(T)$ is known, an independent determination of E_b along $v_c(T)$ since we know its left-hand side from

$$\left.\frac{\partial\ln\Gamma(T,v)}{\partial T}\right|_v=\frac{d\ln\Gamma_c}{dT}-A\frac{dv_c}{dT}.$$

From a mathematical point of view, Eqs. (36) and (37) are equivalent. But the temperature dependence of E_b can be neglected since it is expected to behave as that of the superfluid density, ρ_s, which is very nearly equal to the fluid density below 0.5 K, and is constant.[92] Putting $\partial E_b/\partial T|_v=0$ brings additional physical input and places constraints on α and $\partial\alpha/\partial T|_v$. Matching the values of E_b obtained from Eqs. (36) and (37) at the high-temperature end of the data, with a variation of α joining smoothly to the determination at the low-temperature end, calls for a value of α around 0.1 at 0.419 K. Both determinations of E_b are displayed in Fig. 11.

These determinations are seen in Fig. 11 to differ fairly significantly at LT. They involve different input experimental data, Eq. (37) utilizing the quantity $A=\partial\ln\Gamma/\partial v|_T$. Also, the numerical differentiation of $\ln\Gamma_c$ and the differentiation of the asymptotic evaluation of f_q are prone to increasing errors,[60] and especially so where they contribute most, that is, close to T_0. In all, the two determinations of E_b in Fig. 11

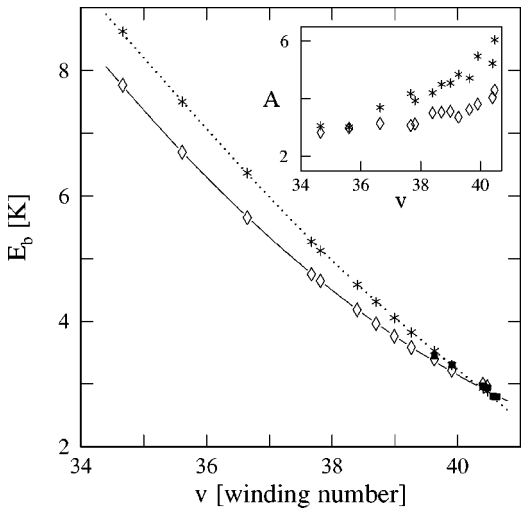

FIG. 12. The barrier energy E_b in kelvin vs v, the velocity in the aperture expressed in winding number (■ and ◇), the same as in Fig. 11; from Eq. (35) assuming ω_0 is constant (∗). The plain curve is a second-order polynomial fit, and the dotted line is a guide for the eye obtained from a cubic spline smoothing routine imposing a rms deviation of 0.02. In the inset are the quantities $A = \partial \ln \Gamma / \partial v|_T$ obtained experimentally (∗); from the derivative of E_b, Eq. (33) (◇).

may not really differ by more than the combined statistical and systematic errors of both experiment and theory.[60]

A third evaluation of E_b can be obtained by integrating $\mathrm{d}E_b/\mathrm{d}v$, given by Eq. (35), starting from the values of E_b and of v_c on the LT plateau. As can be seen in Fig. 12, this third evaluation of E_b lies above the first one because the slope around T_0 is a great deal steeper. A comparison between the measured quantity $A = \partial \ln \Gamma / \partial v|_T$ and $-(1/T)\mathrm{d}E_b/\mathrm{d}v$ as derived from Eq. (36) is shown in the inset. Another illustration of this discrepancy is given in Fig. 9, which shows both the measured width and the width calculated from the final values of the analysis.

The discrepancy between these two quantities is too large to be explained by the experimental uncertainty on A. This last quantity is the slope of $\ln \Gamma$ vs v, as illustrated in Fig. 6: systematic errors coming from extraneous noise sources would broaden the critical transition and would cause A to be too small while the observed discrepancy corresponds to an overestimate of A. The determination of the same quantity derived from the rms spread in v_a is not prone to the same biases in the analysis. As can be seen in Table I, it is on average slightly larger (by approximately 10%) than that stemming directly from $\ln \Gamma$, which makes matters even worse.

A knee-jerk reaction is to call into question the assumption that ω_0 remains constant. As a matter of fact, this quantity does depend on the control parameter v. Lifshitz and Kagan[93] have pointed out on general grounds that $\omega_0 \to 0$ close to the lability point because $\partial^2 V(q)/\partial q^2$ vanishes while the particle mass remains finite (a finite-size vortex ends up being nucleated). More specifically, for analytic potentials, which reduce to the cubic potential (6) close to the lability point, and that depend linearly on v, such as, for instance, for electrodynamic Josephson junctions[26] or vortex nucleation,[4,83] one obtains $q_b = q_0 \nu$, $E_b = E_0 \nu^3$, and $\omega_0^2 = (6E_0/mq_0^2)\,\nu^{1/2}$ with $\nu = (1 - v^2/v_{c0}^2)^{1/2}$, v_{c0} being the velocity at which the system becomes labile.

Attempts to reduce the discrepancy shown in Fig. 12 between the direct determination of E_b and that based on the integral of TA with respect to v, allowing for a dependence of ω_0 on v, do not lead to a realistic functional dependence: ω_0 has to be *reduced* by a factor of 5 between T_0 and 0.4 K while the previous discussion suggested that a moderate *increase* was to be expected.

With the hindsight provided by the half-ring nucleation model,[4] we realize that the assumption $\omega_0 = \omega_b$ must be abandoned and that both quantities must have different dependencies on v. As v decreases and the potential well becomes deeper, the barrier becomes broader and $\partial^2 V(q)/\partial q^2$ decreases while the vortex mass m increases with the nucleated vortex half ring having a larger radius: ω_b is expected to decrease. Using the simplified expression (4) for $\ln f_{\mathrm{th}}$ and keeping ω_0 constant, the variation of ω_b is given by

$$\left[\frac{\alpha}{\sqrt{1+\alpha^2}} + \frac{1}{12}\left(\frac{\hbar\omega_b}{k_B T}\right)^2\right]\frac{1}{\omega_b}\frac{\mathrm{d}\omega_b}{\mathrm{d}v} = A - \frac{1}{k_B T}\frac{\mathrm{d}E_b}{\mathrm{d}v}.$$

Solving numerically for ω_b, we find that a sevenfold or so decrease of ω_b is needed to account for the discrepancy in Fig. 12.

This result indicates clearly that the cubic potential with a fixed mass particle provides only a first approximation to the vortex nucleation problem. A more refined analysis should retain the distinction between ω_0 and ω_b both above and below T_0 but (i) the corresponding theory has not yet been worked out, and (ii) it adds to the number of unknowns, for the determination of which the available experimental input is already too scant.

D. Friction in the nucleation process

The damping coefficient $\alpha = 1/2\omega_b\tau$ is found from experiment to be extremely small below $T_0/2$ but rapidly increasing in the vicinity of T_0. Damping is fairly well determined in this temperature range.

In contrast, thermal activation is only weakly affected by damping, provided that it is neither too strong nor too weak. In both cases the rate is depressed, or, for an experimentally given value of the rate, the energy barrier is lowered. The decrease is slow. For large dissipation, E_b varies as $-\ln \alpha$ according to Eq. (36); for very small dissipation, the depopulation factor Υ (10) becomes proportional to α.[22] Both cases of very large and very small dissipation are excluded by the comparison between Eqs. (36) and (37).

In the intermediate regime, $0.05 < \alpha < 1$, $\ln \Gamma$ exhibits a broad maximum which does not allow to pinpoint the value of α. Also, letting ω_0 (and ω_b) depend on v brings additional indetermination. A value of 0.1 for α at 0.419 K minimizes the difference between the determinations of E_b from Eq. (36) and from the integral $\int TA\,\mathrm{d}v$ shown in Fig. 12. By the same token, the variation of ω_b with v is also kept to a minimum.

Apart from the classic case of the electrodynamic Josephson junction,[94,95] which can be well modeled by an electrical circuit, little is known about dissipation in the nucleation of mesoscopic objects. The motion of vortices in helium is impeded by mutual friction, caused at LT by the collision with ballistic phonons. Phonon scattering on a vortex filament leads to the following force:[96,97]

$$\vec{F} = 10.8 \frac{(k_B T)^5}{m_4^2 c^7 \hbar^2} \vec{u} + 8.24 \frac{(k_B T)^4}{\pi m_4 c^5 \hbar^2} \vec{u} \times \hat{\kappa}, \qquad (38)$$

in which c is the velocity of first sound, $\vec{u}$ the vortex velocity with respect to the normal fluid, and $\hat{\kappa}$ the unit vector along the vorticity. The evaluation of Eq. (38) for a half-ring vortex of diameter $d = 30$ Å and mass $M \sim 20 m_4$ leads to $\alpha = \pi F d / 2 \omega_b M u = 3.6 \times 10^{-5} T^5$, a negligible quantity.

However, the mechanism leading to Eq. (38) is not the most relevant because the vortex size is of the order of the dominant phonon wavelength; the structure of the vortex, namely, its eigenmodes of deformation, plays an important role. The eigenmode frequencies of a full ring are expressed by[98]

$$\omega_n = \frac{\hbar n \sqrt{n^2 - 1}}{2 m_4 R^2} \ln \frac{R}{a_0},$$

in which a_0 is the vortex core radius. The friction force is proportional to the number density of phonons which can excite these modes. The first nonzero eigenmode ($n = 2$) represents an elliptical deformation and also exists for the half-ring vortex. It gives the dominant contribution to α, $\propto (\exp\{\hbar \omega_2 / k_B T\} - 1)^{-1}$, in which $\omega_2 = 0.215$ K with $R = d/2 = 15$ Å. The values of α collected in Table II correspond to $0.082/(\exp\{0.25/T\} - 1)$, which yields $\alpha = 0.1$ at 0.419 K and fits best the values of $\ln \Gamma(v_q)$ obtained with the smoothed v_c also collected in Table II (see the inset of Fig. 10).

The three last columns of Table II contain the values of the quantum corrections $\ln f_q$, of the depopulation factor $\ln \Upsilon$, and of the energy barrier E_b that result from this analysis. The quantum corrections play a major role about T_0. The depopulation factor remains close to 1: the plateau of v_c is very far from being due to a loss of thermal contact of the nucleating entity with its environment.

E. Universality

The results in Table II pertain to a particular, well-studied, aperture.[99] Different runs with different ^{4}He samples, pure and less pure, in the same aperture, at pressures close to SVP, all show the same well-defined LT plateau setting in at the same temperature, although the mean velocity in the aperture may differ by a few percent, as in Fig. 8, or more, as for the data on the 100-ppb sample shown in Fig. 5. The width also shows variations, as seen in Fig. 9.

These changes are believed to be due to contamination by solidified gases that takes place on nanometric scales, and therefore, affects the nucleation site geometry. Contamination on a larger scale, a few tens of nanometers, leads to a profound modification of the peak amplitude charts, as reported in Refs. 7, 100 and 101. Heavy contamination on an even larger scale, such as to partially block the aperture, is unlikely in these experiments since the gas samples were always extremely well purified and the experimental cell carefully flushed with the purified gas. It follows from these remarks that the results in Table II, established for the set of experimental runs reported here, may be expected to vary from experiment to experiment, as is indeed seen in Figs. 8 and 9. We note that T_0 and the nucleation rate itself are little affected by these changes, as seen in Figs. 8 and 10.

Vortex nucleation rates in apertures have also been measured by Zimmermann, Jr. *et al.*[102] and by Steinhauer *et al.*[73,103,104] These authors have measured the phase-slip rate by ramping up the pressure head applied to the aperture, using the phase-slippage cell off resonance in a nonresonant, "*dc*" mode. Slip rates can be turned into energy barriers with the help of Eq. (36), and pressure heads into aperture velocities with that of the Euler equation. We have translated the slip rate data of Refs. 73 and 103 into energy barrier values using the same ω_0 and $\alpha(T)$ as for Table II. The outcome is shown in Fig. 13 as ragged strips. Davis *et al.* have also used earlier resonator data[49] of the type described here, which are also plotted in Fig. 13. The straight segments attached to each data point, marked with asterisks, represent dE_b/dv as obtained from the critical transition width.

The velocity scale in Fig. 13 is based on a normalization of velocities to the linearly extrapolated value at $T = 0$. This scale is somewhat uncertain since the linear dependence of v_c on T does not extend to temperatures below ~ 0.3 K. One way to bring the two sets of resonator data marked by diamonds and asterisks in Fig. 13 into semiquantitative agreement is to adjust, as was done in Ref. 105, the velocity scale by $\sim 15\%$ and to use the value for T_0—0.20 K—quoted by Davis *et al.*[49] Another way would be to move the asterisks in Fig. 13 upward by adjusting ω_0 at each temperature. The necessary adjustment—at 0.66 K for instance, an upward shift by ~ 6.5 K—would lead to an increase of ω_0 by a rather large factor of 10^4. Either way, the necessity of such adjustments makes the universal character of $E_b(v)$ obtained from the resonator data a matter of debate.

The dc data, marked by the ragged traces, would require even larger adjustments of ω_0 and are for their part definitely off track. In particular, the effective energy barrier at large pressure heads does not decrease rapidly enough as v increases to extrapolate to zero as v_c increases. We refer to Ref. 105 for a possible explanation of these anomalies at large slip rates based on a backflow effect of the emitted vortices on the nucleation site.

The results of Zimmermann, Jr. *et al.*[102] follow roughly the same pattern as those of Steinhauer *et al.*[73,103] The authors of Ref. 102 used a larger aperture and smaller pressure heads; their data are less prone to backflow corrections. Nonetheless, the energy barriers that can be derived from their data are lower than in the present work, again showing that site-to-site differences exist in the nucleation of vortices.

The discrepancy between the resonator data and the dc data in Refs. 73 and 103 has also been noted by Niemetz and Schoepe.[74] These authors reanalyzed the dc results of Stein-

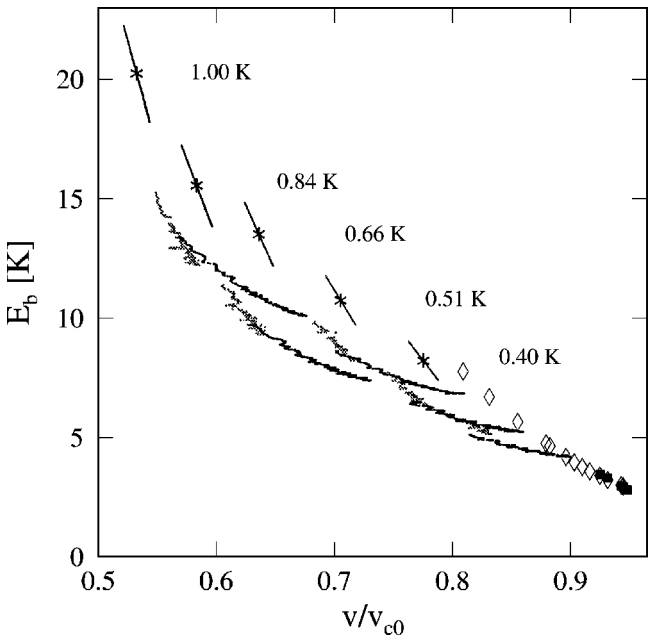

FIG. 13. The barrier energy E_b in kelvin vs v/v_{c0}, the velocity in the aperture normalized to the linearly extrapolated value at $T=0$: from Table II (■ and ◇); nucleation rate data from Refs. 73 and 103 at various temperatures, converted to energy barriers as described in the text (∗), and continous ragged traces.

hauer *et al.* from different premises[106] and obtained a curve similar to the strip of traces in Fig. 13. This strip lies significantly below the resonator data points, and, consequently, the corresponding attempt frequency is lower. Niemetz and Schoepe found a value of $\omega_0/2\pi$ of 1.2×10^4 Hz,[106] much lower than the value considered here, 1.9×10^{10} Hz, given by Eq. (5) with $T_0=0.144$ K.

Also, the onset temperature for the quantum plateau reported by Davis *et al.*[49] is about 200 mK, 50% higher than the temperature reported here. The crossover temperature reported by Hendry *et al.*,[47] at which the nucleation rate saturates in ion propagation experiments, a rather different instance of vortex nucleation, lies at around 200 to 240 mK. In terms of the corresponding attempt frequencies, these different figures lie at in the same range. It is nonetheless rather puzzling that the two aperture-flow experiments do not lie closer to one another since the critical velocities at the nucleation site are presumably comparable (20 to 30 m/s) and much smaller than for ion propagation (about 60 m/s); the nucleated vortex is more than twice smaller in the latter case.

To conclude, we point out that, in spite of differences in experimental setups and data reduction methods, the various data display similar trends. Quantitative agreement is not achieved, and energy barriers are hardly ''universal,'' but not to the point of casting doubt on the fact that the underlying mechanism for phase slip nucleation in these different instances is the same.

The present results, given in Table II, possess full consistency between the high- and low-temperature behaviors with a value of the attempt frequency given by the crossover temperature between these two behaviors. The values for E_b and $\omega_0/2\pi$ obtained here certainly fall into physically plausible ranges, the latter being of the order of the highest Kelvin mode frequency, the former being of the order of the energy of vortices large enough to survive in the locally applied flow field of 10 to 20 m/s.

F. Nucleation sites

Our present knowledge of nucleation sites for vortices is at best rudimentary and we are left to conjecture as to how these sites exactly appear. Experiments aimed at ascertaining the effect of aperture geometry have led to puzzling results.[107] The common belief is that they must consist of nanometer-size defects, either geometrical or chemical, at the aperture wall.

The above nucleation model and analysis rest on the assumption that one given Brownian particle escapes at a time from a well-defined potential well. As noted on heuristic grounds by Schoepe,[108] there can, in principle, exist a large multiplicity of nearly equivalent nucleation sites at the walls of the microaperture. Acting independently of one another, they would impress their own statistical distribution of properties on the measured nucleation rate, foiling the analysis of Sec. III.

We argue on two grounds that such is not the case and that a primary site is involved. Let us first consider the structure of the aperture walls and the superfluid flow past them. The aperture is micromachined by ion bombardment or by chemical etching. These processes are similar to diffusion front propagation and create interfaces with a fractal character:[109] height fluctuations of the interface may be expected to display a fractional Brownian pattern with a $1/f^{\alpha}$ spectrum extending from atomic dimensions to sizes comparable with that of the aperture. This fractal nature renders the various possible nucleation sites inequivalent to one another by a large extent, some being lean, some being fat. Potential flow of the superfluid picks up the spikiest, on a nanometer scale, of these sites, located on the most prominent large scale defect. Given the scarcity of sites in high flow regions, the next most favorable one is likely to be much less effective: there is but one Mount Everest on Earth; K2 is 2.7% shorter.

The peak amplitude chart, Fig. 2, provides another clue, based on experiment. If there were a number of nearly equivalent, uncorrelated nucleation sites, multiple slips would occur with a random pattern characteristic of the superposition of Gaussian processes, quite unlike that in Fig. 2. In particular, multiple slips occur predominantly in a preferential flow direction (fostering minus slips), and their frequency varies with temperature and ^{3}He impurity content. More properties of multiple slips and flow collapses are described in Refs. 69 and 81. They do not appear to be a signature of multiple nucleation sites; a possible mechanism for their occurrence is discussed in Ref. 55.

It still remains possible that a secondary site would play second fiddle to the primary one, causing a slip now and then. This possibility would not be easily spotted on the peak amplitude charts. Corresponding to a less frequent event, it would not distort significantly the slip probability, but, if really present, it would *raise* the apparent value of A and help explain the discrepancy in Fig. 12.

VI. SUMMARY

We have given a detailed account of how the slip nucleation rate is obtained from phase-slippage experiments. The knowledge of the nucleation rate in ultrapure ^{4}He at various temperatures and velocities leads to that of v_c and Δv_c. These quantities compare satisfactorily to those extracted from the mean velocity v_a and its rms fluctuations; the (small) discrepancies place confidence limits on the results.

The experimental data display two regimes: a temperature-independent plateau below ~ 120 mK, and a thermal regime above, which are interpreted in terms of quantum-tunneling nucleation and thermally assisted nucleation. Using theoretical results established for the escape of a particle trapped in a potential well and subjected to random forces from its environment, we have extracted the values of the confining energy barrier at various temperatures (and velocities) as well as the attempt frequency. The analyses of the LT and high-T data, and their comparison, lead to the following results:

(i) The LT data yield both the value of E_b in the limit $T \to 0$ and the attempt frequency. The resulting crossover temperature is $T_0 = 0.144$ K.

(ii) The analysis of the high-T data has been conducted in different ways which show that the energy barrier and the attempt frequency determined from the high-T data are compatible with those determined from the LT plateau.

(iii) The nucleation model parameters can be tailored to rather precisely fit the data. The fine touches lead to an estimate of damping, which is vanishingly small below $T_0/2$, and increases above, rapidly at first to above T_0, and then moderately. The anomalously sharp break between the quantum plateau and the thermal regime is thus explained.

(iv) Further improvement of the consistency between the nucleation model and the high-temperature data calls for a refinement of the potential-well shape and for due accounting of the mass of the tunneling vortex.

These results leave little room for doubt that vortices in aperture flow are nucleated by thermal activation above ~ 0.15 K, and by quantum tunneling below, with an energy barrier as low as 3 K at 0.15 K and an attempt frequency of $\sim 2 \times 10^{10}$ Hz. No other vortex creation mechanism need be invoked to explain the LT plateau. We have argued that the disruptive takeover by a different mechanism, involving, e.g., solitons or bubbles, would lead to a different behavior of v_c and Δv_c. Damping, albeit small, plays a significant role in the crossover region: superfluid helium thus provides another system, besides Josephson junctions, in which the effect of dissipation on the tunneling of mesoscopic objects can be studied.

ACKNOWLEDGMENTS

Seeds for this work, which benefited from stimulating discussions with Yu. Mukharsky and W. Zimmermann, Jr., were sown at the Workshop on Vortex Dynamics and Quantum Turbulence held at the Newton Institute in Cambridge in August 2000, attended by E.V. The authors thank Wilfried Schoepe for informing them of his work prior to publication and Hermann Grabert for useful correspondence. The help of Gary Ihas during the setting up of the experiment and the measurements, and that of Ronald Aarts for the early data analysis, is gratefully acknowledged.

*Email address: evaroquaux@cea.fr
†Email address: oavenel@cea.fr

[1] R.P. Feynman, *Progress in Low Temperature Physics*, edited by C.J. Gorter (North-Holland, Amsterdam, 1955), Vol. 1, p. 36.
[2] S. Burkhart, M. Bernard, O. Avenel, and E. Varoquaux, Phys. Rev. Lett. **72**, 380 (1994).
[3] W. Zimmermann, Jr., J. Low Temp. Phys. **91**, 219 (1993).
[4] O. Avenel, G.G. Ihas, and E. Varoquaux, J. Low Temp. Phys. **93**, 1031 (1993).
[5] E. Varoquaux and O. Avenel, Physica B **197**, 306 (1994).
[6] W. Zimmermann, Jr., Contemp. Phys. **37**, 219 (1996).
[7] E. Varoquaux, in *Topological Defects and the Non-Equilibrium Dynamics of Symmetry Breaking Phase Transitions*, edited by Y.M. Bunkov and H. Godfrin (Kluwer Academic, Dordrecht, 2000), p. 303.
[8] K.W. Schwarz, Phys. Rev. B **31**, 5782 (1985).
[9] *Quantized Vortex Dynamics and Superfluid Turbulence*, edited by C.F. Barenghi, R.J. Donnelly, and W.F. Vinen (Springer-Verlag, Berlin, 2001).
[10] G.G. Ihas, O. Avenel, R. Aarts, R. Salmelin, and E. Varoquaux, Phys. Rev. Lett. **69**, 327 (1992).
[11] S.V. Iordanskii, Zh. Éksp. Teor. Fiz. **48**, 708 (1965) [Sov. Phys. JETP **21**, 467 (1965)].
[12] J.S. Langer and M.E. Fisher, Phys. Rev. Lett. **19**, 560 (1967).
[13] G.E. Volovik, Pis'ma Zh. Éksp. Teor. Fiz. **15**, 116 (1972) [JETP Lett. **15**, 81 (1972)].
[14] C.M. Muirhead, W.F. Vinen, and R.J. Donnelly, Philos. Trans. R. Soc. London, Ser. A **311**, 433 (1984).
[15] E.B. Sonin, Zh. Éksp. Teor. Fiz. **64**, 970 (1973) [Sov. Phys. JETP **37**, 494 (1973)].
[16] E.B. Sonin, Physica B **210**, 234 (1995).
[17] U.R. Fischer, Phys. Rev. B **58**, 105 (1998); **63**, 229902(E) (2001).
[18] U.R. Fischer, Physica B **255**, 41 (1998).
[19] V.I. Goldanski, Dokl. Akad. Nauk SSSR **124**, 1261 (1959); **127**, 1037 (1959).
[20] I. Affleck, Phys. Rev. Lett. **46**, 388 (1981).
[21] J. Clarke, A.N. Cleland, M.H. Devoret, D. Estève, and J.M. Martinis, Science **239**, 992 (1988).
[22] H. Kramers, Physica (Amsterdam) **7**, 284 (1940).
[23] J.S. Langer, Ann. Phys. (N.Y.) **41**, 108 (1967).
[24] A.O. Caldeira and A.J. Leggett, Ann. Phys. (N.Y.) **149**, 374 (1983); **153**, 445(E) (1984).
[25] J.M. Martinis and H. Grabert, Phys. Rev. B **38**, 2371 (1988).
[26] A. Larkin, K.K. Likharev, and Yu.N. Ovchinnikov, Physica B **126**, 414 (1984).
[27] H. Grabert, in *SQUID'85—Superconducting Quantum Interference Devices and their Aplications*, edited by H. Hahlbolm and H. Lübbig (de Gruyter and Company, Berlin, 1985), p. 289.
[28] P. Hänggi, P. Talkner, and M. Borkovec, Rev. Mod. Phys. **62**, 251 (1990).
[29] V.I. Mel'nikov, Phys. Rep. **209**, 1 (1991).

[30] R.F. Voss and R.A. Webb, Phys. Rev. Lett. **47**, 265 (1981).
[31] M.H. Devoret, J.M. Martinis, D. Estève, and J. Clarke, Phys. Rev. Lett. **53**, 1260 (1984).
[32] J.M. Martinis, M.H. Devoret, and J. Clarke, Phys. Rev. Lett. **55**, 1543 (1985).
[33] M.H. Devoret, J.M. Martinis, and J. Clarke, Phys. Rev. Lett. **55**, 1908 (1985).
[34] R.E. Thorne, J.H. Miller, W.G. Lyons, J.W. Lyding, and J.R. Tucker, Phys. Rev. Lett. **55**, 1006 (1985).
[35] J. Bardeen, Phys. Rev. B **39**, 3528 (1989).
[36] G. Blatter, V.B. Geshkenbein, and V.M. Vinokur, Phys. Rev. Lett. **66**, 3297 (1991), and references to the experimental work therein.
[37] L. Fruchter, A.P. Malozemoff, I.A. Campbell, J. Sanchez, M. Konczykowski, R. Griessen, and F. Holtzberg, Phys. Rev. B **43**, 8709 (1991).
[38] D.M. Stamper-Kurn, H.-J. Miesner, A.P. Chikkatur, S. Inouye, J. Stenger, and W. Ketterle, Phys. Rev. Lett. **83**, 661 (1999).
[39] H.P. Büchler, V.B. Geshkenbein, and G. Blatter, in *Quantized Vortex Dynamics and Superfluid Turbulence* (Springer-Verlag, Berlin, 2001), p. 334.
[40] H. Maris, J. Low Temp. Phys. **98**, 403 (1995).
[41] H. Lambaré, P. Roche, S. Balibar, H.J. Maris, O.A. Andreeva, C. Guthmann, K.O. Keshishev, and E. Rolley, Eur. Phys. J. B **2**, 381 (1998).
[42] S. Balibar, F. Caupin, H. Lambaré, P. Roche, and H.J. Maris, J. Low Temp. Phys. **113**, 459 (1998); S. Balibar, *ibid.* **129**, 363 (2002).
[43] J.P. Ruutu, P.J. Hakonen, J.S. Penttilä, A.V. Babkin, J.P. Saramäki, and E.B. Sonin, Phys. Rev. Lett. **77**, 2514 (1996).
[44] E.M. Chudnovsky and L. Gunther, Phys. Rev. Lett. **60**, 661 (1988).
[45] B. Barbara and E.M. Chudnovsky, Phys. Lett. A **145**, 205 (1990).
[46] C.M. Muirhead, W.F. Vinen, and R.J. Donnelly, Proc. R. Soc. London, Ser. A **402**, 225 (1985).
[47] P.C. Hendry, N.S. Lawson, P.V.E. McClintock, C.D.H. Williams, and R.M. Bowley, Phys. Rev. Lett. **60**, 604 (1988).
[48] R.E. Packard and S. Vitale, Phys. Rev. B **45**, 2512 (1992).
[49] J.C. Davis, J. Steinhauer, K. Schwab, Yu. Mukharsky, Ajay Amar, Y. Sasaki, and R.E. Packard, Phys. Rev. Lett. **69**, 323 (1992).
[50] R.L. Davis, Physica B **178**, 76 (1992).
[51] G.E. Volovik, Pisma Zh. Éksp. Teor. Fiz. **65**, 201 (1997) [JETP Lett. **65**, 217 (1997)].
[52] R.N. Hills and P.H. Roberts, J. Phys. C **11**, 4485 (1978).
[53] N.G. Berloff and P.H. Roberts, in *Quantized Vortex Dynamics and Superfluid Turbulence* (Springer-Verlag, Berlin, 2001), p. 268.
[54] E. Varoquaux, G.G. Ihas, O. Avenel, and R. Aarts, J. Low Temp. Phys. **89**, 547 (1992).
[55] E. Varoquaux, O. Avenel, Yu. Mukharsky, and P. Hakonen, in *Quantized Vortex Dynamics and Superfluid Turbulence* (Springer-Verlag, Berlin, 2001), p. 36.
[56] H. Grabert, P. Olschowski, and U. Weiss, Phys. Rev. B **36**, 1931 (1987).
[57] D. Waxman and A.J. Leggett, Phys. Rev. B **32**, 4450 (1985).
[58] T. Frisch, Y. Pomeau, and S. Rica, Phys. Rev. Lett. **69**, 1644 (1992).
[59] C. Nore, C. Huepe, and M.E. Brachet, Phys. Rev. Lett. **84**, 2191 (2000).
[60] The quantum correction close to T_0, f_{co}, is evaluated analytically in the limit of a high energy barrier in Ref. 56, which is not the case here since $E_b/\hbar\omega_0 \sim 3$. This leads to numerical inaccuracies [H. Grabert (private communication)]. These inaccuracies turn out to be large in the determination of the partial derivatives of f_{co} with respect to T and v which are needed in Sec. V. In particular, the accuracy of the evaluation of Eq. (37) in the crossover regime is questionable.
[61] H. Grabert, Phys. Rev. Lett. **61**, 1683 (1988).
[62] E. Pollak, Phys. Rev. A **33**, 4244 (1986).
[63] I. Rips and E. Pollak, Phys. Rev. A **41**, 5366 (1989).
[64] D. Esteve, M.H. Devoret, and J.M. Martinis, Phys. Rev. B **34**, 158 (1986).
[65] K.S. Chow, D.A. Browne, and Vinay Ambegaokar, Phys. Rev. B **37**, 1624 (1988).
[66] O. Avenel and E. Varoquaux, Jpn. J. Appl. Phys., Part 1 **26**, 1798 (1987).
[67] B.P. Beecken and W. Zimmermann, Jr., Phys. Rev. B **35**, 1630 (1987).
[68] E. Varoquaux, O. Avenel, and M. Meisel, Can. J. Phys. **65**, 1377 (1987).
[69] O. Avenel, M. Bernard, S. Burkhart, and E. Varoquaux, Physica B **210**, 215 (1995).
[70] O. Avenel, P. Hakonen, and E. Varoquaux, J. Low Temp. Phys. **110**, 709 (1998).
[71] O. Avenel, P. Hakonen, and E. Varoquaux, Phys. Rev. Lett. **78**, 3602 (1997).
[72] W. Zimmermann, Jr., O. Avenel, and E. Varoquaux, Physica B **165&166**, 749 (1990).
[73] J. Steinhauer, K. Schwab, Yu. Mukharsky, J.C. Davis, and R.E. Packard, J. Low Temp. Phys. **100**, 281 (1995).
[74] N. Niemetz and W. Schoepe, J. Low Temp. Phys. **126**, 805 (2002).
[75] E. Varoquaux, G.G. Ihas, O. Avenel, and R. Aarts, Phys. Rev. Lett. **70**, 2114 (1993).
[76] E. Varoquaux, W. Zimmermann, Jr., and O. Avenel, *Excitations in Two-Dimensional and Three-Dimensional Quantum Fluids*, edited by A.F.G. Wyatt and H.J. Lauter (Plenum, New York, 1991), p. 343.
[77] M. Born and E. Wolf, *Principles of Optics*, 3rd ed. (Pergamon, Oxford, 1965), p. 747.
[78] E. Varoquaux, M.W. Meisel, and O. Avenel, Phys. Rev. Lett. **57**, 2291 (1986).
[79] See, for instance, the *Handbook of Mathematical Functions*, edited by M. Abramowitz and I. Stegun (Dover, New York, 1965), Chap. V.
[80] O. Avenel and E. Varoquaux, Czech. J. Phys. **46-S6**, 3319 (1996).
[81] E. Varoquaux, O. Avenel, M. Bernard, and S. Burkhart, J. Low Temp. Phys. **101**, 821 (1995).
[82] In the caption of Fig. 2 of Ref. 55, the cumulative probability P was mistakenly referred to as p.
[83] J.S. Langer and J.D. Reppy, *Progress in Low Temperature Physics*, edited by C.J. Gorter (North-Holland, Amsterdam, 1970), Vol. 6, Chap. 1.
[84] R.M. Bowley, J. Low Temp. Phys. **87**, 137 (1992).
[85] M.H. Devoret, J.M. Martinis, and J. Clarke, Phys. Rev. Lett. **63**, 212 (1989).
[86] A. Garg, Phys. Rev. Lett. **70**, 2198 (1993).
[87] L. Fruchter, I.A. Campbell, and M. Konczykowski, Phys. Rev. Lett. **72**, 791 (1994).

[88] Yu. Mukharsky, O. Avenel, and E. Varoquaux, Physica B **280**, 287 (2000).
[89] C. Josserand and Y. Pomeau, Europhys. Lett. **30**, 43 (1995).
[90] C. Josserand, Y. Pomeau, and S. Rica, Phys. Rev. Lett. **75**, 3150 (1995).
[91] K.W. Schwarz, Phys. Rev. Lett. **64**, 1130 (1990).
[92] Below 0.5 K, phonons give the dominant contribution to the normal fluid fraction $\rho_n/\rho \sim 1.6\times 10^{-4}T^4$, and to the temperature dependence of the total fluid density ρ. The variation of ρ_s with temperature is mainly due to that of ρ, the thermal expansion of the fluid varying as $1.1\times 10^{-3}T^3$ K^{-1} [K.R. Atkins and M.H. Edwards, Phys. Rev. **97**, 1429 (1955)]. The correction to E_b is -0.5×10^{-3} K at 0.5 K, and decreasing with T^3 below.
[93] I.M. Lifshitz and Yu. Kagan, Zh. Éksp. Teor. Fiz. **62**, 385 (1972) [Sov. Phys. JETP **35**, 206 (1972)].
[94] P. Silvestrini, S. Pagano, R. Cristiano, O. Liegme, and K.E. Gray, Phys. Rev. Lett. **83**, 661 (1988).
[95] E. Turlot, D. Estève, C. Urbina, J.M. Martinis, M.H. Devoret, S. Linkwitz, and H. Grabert, Phys. Rev. Lett. **62**, 1788 (1989).
[96] L.P. Pitaevskii, Zh. Éksp. Teor. Fiz. **35**, 1271 (1958) [Sov. Phys. JETP **8**, 888 (1959)].
[97] S.V. Iordanskii, Zh. Éksp. Teor. Fiz. **49**, 225 (1965) [Sov. Phys. JETP **22**, 160 (1966)].
[98] J.J. Thomson (1893), as quoted by S.E. Widnall and J.P. Sullivan, Proc. R. Soc. London, Ser. A **332**, 335 (1973).
[99] The microaperture used in these experiments is the nominally 0.3×5-μm slit ion-drilled in a 0.2-μm-thick nickel foil used in other experiments in our laboratory. Its manufacture is described by P. Sudraud, P. Ballongue, E. Varoquaux, and O. Avenel, J. Appl. Phys. **62**, 2163 (1987). This aperture was permanently contaminated by a 20- to 40-nm-thick layer of amorphous carbon before ever being used during inspection under a transmission electron microscope to determine its exact size.
[100] P. Hakonen, O. Avenel, and E. Varoquaux, Phys. Rev. Lett. **81**, 3451 (1998).
[101] E. Varoquaux, O. Avenel, P. Hakonen, and Yu. Mukharsky, Physica B **255**, 55 (1998).
[102] W. Zimmermann, Jr., C.A. Lindensmith, and J.A. Flaten, J. Low Temp. Phys. **110**, 497 (1998).
[103] J. Steinhauer, K. Schwab, Yu.M. Mukharsky, J.C. Davis, and R.E. Packard, Phys. Rev. Lett. **74**, 5056 (1995).
[104] J. Steinhauer, S. Backhaus, and R.E. Packard, Phys. Rev. B **52**, 9654 (1995).
[105] E. Varoquaux and O. Avenel, Phys. Rev. Lett. **76**, 1180 (1996).
[106] The authors of Ref. 74 assume, in particular, that the transition width Δv_c is independent of temperature. While this assumption seems justified in the vicinity of 0.6–0.8 K where $\Delta v_c(T)$ has a maximum, it is not borne out by the low-temperature data in Fig. 9 nor at $T \gtrsim 1$ K [see Zimmermann, Jr. *et al.* (Ref. 102)]. This remark affects the analytical form of E_b proposed in Ref. 74 but not the values found for E_b and the attempt frequency.
[107] G.M. Shifflett and G.B. Hess, J. Low Temp. Phys. **98**, 591 (1995).
[108] W. Schoepe, Physica B **329-333**, 195 (2003).
[109] J.-F. Gouyet, *Physics and Fractal Structures* (Masson, Paris, 1996).